Reconstruction of Voronoi diagrams: the case of inverse conductivity problems*

Ernesto G. Birgin† Antoine Laurain‡ Danilo R. Souza§

November 19, 2024¶

Abstract

In this work, we present and analyze a numerical method for recovering a piecewise constant conductivity with multiple phases in inverse conductivity problems. Specifically, we consider two types of inverse conductivity problems: problems with boundary measurements or with internal measurements. The conductivity is assumed to be constant in each phase, and a Voronoi diagram generated by a set of sites is used to model the phases. An optimization problem with respect to the position of the sites is described to approximate the solution of the inverse problem. Combining techniques from non-smooth shape calculus and the sensitivity of Voronoi diagrams, we prove shape differentiability and compute the gradient of the cost function. Two different formulas for the gradient, a volumetric one and an interface one, are provided. The dependence of the reconstruction on the problem parameters, such as noise, number of sites, and initialization, is investigated through several numerical experiments.

Keywords: Inverse conductivity problems, non-smooth shape calculus, Voronoi diagrams, optimization.

AMS subject classifications: 49Q10, 49J52, 49Q12.

1 Introduction

Identifying the scalar conductivity coefficient of a second-order elliptic equation in divergence form posed on a bounded domain is a well-established problem, with numerous variations and a large body of literature devoted to it; see [32, 47]. In this paper, we consider two types of inverse conductivity problems: electrical impedance tomography (EIT), which involves boundary measurements, and an inverse conductivity problem with internal measurements. Firstly, EIT, also known as inverse conductivity or Calderón's problem, has been intensively studied and applied since the 1980s; see [17] for a thorough review of the topic. The purpose of EIT is to reconstruct the electrical conductivity within a medium using boundary measurements of the electrical potential obtained by applying boundary currents. It is a low-cost, noninvasive, radiation-free, and portable imaging technique with applications in medical imaging, geophysics, civil engineering, and nondestructive testing. Second, the inverse conductivity problem with internal measurements has applications in the so-called coupled physics or hybrid imaging modalities, which combine the best imaging properties of different types of waves used in medical imaging. The stability of the solution of this inverse problem has been studied, and numerical resolution algorithms have been proposed in [2, 5, 46]. Error estimates for the approximate identification of the conductivity

*This work has been partially supported by FAPESP (grants 2013/07375-0, 2022/05803-3, 2022/16733-6, and 2023/08706-1) and CNPq (grant 302073/2022-1). Antoine Laurain also acknowledges the support, since May 2023, of the Collaborating Researcher Program of the Institute of Mathematics and Statistics at the University of São Paulo.

†Department of Computer Science, Institute of Mathematics and Statistics, University of São Paulo, Rua do Matão, 1010, Cidade Universitária, 05508-090, São Paulo, SP, Brazil. e-mail: egbirgin@ime.usp.br. Corresponding author.

‡Faculty of Mathematics, University of Duisburg-Essen, Thea-Leymann-Str. 9, 45127, Essen, Germany, e-mail: antoine.laurain@uni-due.de

§Department of Applied Mathematics, Institute of Mathematics and Statistics, University of São Paulo, Rua do Matão, 1010, Cidade Universitária, 05508-090, São Paulo, SP, Brazil. e-mail: danilogyn01@gmail.com

¶Revision made on March 24, 2025.

using the least-squares fitting of the observed data have been obtained in [20]. The convergence rates for the Tikhonov regularization of the identification problem have been obtained in [24]. Also, under appropriate conditions, this problem can be treated as a first-order hyperbolic equation in the unknown coefficient, see [44].

In the literature on inverse conductivity problems, conductivity is often assumed to be a relatively smooth, continuous function. However, the case where the conductivity has discontinuities is important for applications, especially in geophysics and civil engineering, but also in medicine. The problem of reconstructing conductivities with sharp interfaces in EIT, also known as the inclusion detection problem, has attracted considerable interest over the last three decades, starting with pioneering work [21]. A variety of numerical methods for the reconstruction of discontinuous conductivities have been developed and applied in the context of EIT, such as the factorization method [25], monotonicity-based shape reconstruction [26], the enclosure method [31], the MUSIC algorithm [4]. Shape optimization [1, 18, 27, 38] and topological derivative-based methods [3, 16, 28, 29] techniques have also been used to solve this problem. The identification of polygonal inclusions, which has similarities with the problem considered in this work, has been studied in [8, 9]. In this work, we follow this path and consider the particular case where the conductivity is a piecewise constant function [28, 38]. The domain of definition of the conductivity can then be divided into cells such that the conductivity is constant in each cell.

The present work is also a continuation of [14], where we considered the reconstruction of a potential coefficient in an elliptic equation. Here we consider a similar framework where the parameter is also piecewise constant on a Voronoi diagram. However, the problem is even more challenging because of the presence of the piecewise-constant parameter in the higher-order term of the PDE. In particular, this leads to stronger singularities in the solution of the PDE, which need to be carefully analyzed, as they are crucial for the proof of shape differentiability. Since the differential operator is the same for both conductivity problems, the two types of inverse problem considered in this work share similar features. In particular, the singularities at the vertices of the diagram are similar. We first present the theoretical framework and results for the EIT problem, followed by a brief explanation of the similar framework for the problem with internal measurements.

The remainder of this paper is organized as follows. In Section 2, the mathematical model for the inverse conductivity problems is presented. In particular, the PDEs and the cost functional are described. In Section 3, essential results for the sensitivity analysis of Voronoi diagrams with PDEs are recalled and adapted to our setting. In Section 4, these results are applied to prove the shape differentiability and to compute the gradient of the cost function for the EIT problem. Both the interface and distributed expressions of the gradient are obtained, which requires a detailed analysis of the regularity of the solution to the underlying PDE. A singular case is also discussed. Section 5 describes similar results in the case of the conductivity problem with internal measurements. In Section 6, the numerical method is described, and several numerical experiments are performed to investigate its properties. Conclusions and lines for future research are given in the last section.

Notation. $\|\cdot\|$ denotes the Euclidean norm. We use $y^\perp$ for the rotation of angle $\pi/2$ of a vector $y \in \mathbb{R}^2$, with respect to a counterclockwise orientation. The identity matrix in $\mathbb{R}^{2\times 2}$ is denoted by I_2.

2 Mathematical model for inverse conductivity problems

We consider inverse problems where the goal is to recover a scalar-valued conductivity $\sigma^\star$ of a body $\mathcal{D} \subset \mathbb{R}^d$ satisfying the elliptic equations

$$\operatorname{div}(\sigma^\star \nabla U_\alpha^\star) = f \text{ in } \mathcal{D}, \tag{1}$$

where $U_\alpha^\star$, $\alpha = 1, \ldots, \bar{\alpha}$, are potentials. We study two types of inverse problems. In the first problem, we take $f \equiv 0$, the potentials are associated with applied boundary current fluxes $g_\alpha = \sigma^\star \nabla U_\alpha^\star \cdot \nu|_{\partial\mathcal{D}}$, where ν denotes a unit normal vector on $\partial\mathcal{D}$, and noisy measurements $h_\alpha \approx U_\alpha^\star|_{\partial\mathcal{D}}$ of boundary voltages $U_\alpha^\star|_{\partial\mathcal{D}}$ are available on $\partial\mathcal{D}$. Alternatively, measurements could be taken on a subset of $\partial\mathcal{D}$. This problem is known as the continuum model in EIT, also known as the Calderón problem; we refer to the reviews [7, 17] and the references therein. In the second problem, called inverse conductivity problem with internal data [2, 46], we take $f \not\equiv 0$, $\bar{\alpha} = 1$, homogeneous Dirichlet boundary conditions $U_1^\star = 0$ on $\partial\mathcal{D}$,

and interior noisy measurements $h \approx U_1^\star|_{\mathcal{D}}$ in $\mathcal{D}$; one could also consider measurements on a subset of $\mathcal{D}$.

In this section, we describe the mathematical model for the EIT problem. The setting for the inverse conductivity problem with internal data is similar and will be described in Section 5. Let $\mathcal{D} \subset \mathbb{R}^2$ be a bounded, Lipschitz, simply connected, and piecewise $\mathcal{C}^1$ domain. For a given ground truth electrical conductivity $\sigma^\star \in L^\infty(\mathcal{D}), \sigma^\star \geq \underline{\sigma} > 0$, and a given set of applied currents $\{g_\alpha\}_{\alpha=1}^{\bar{\alpha}}$, $g_\alpha \in L^2(\partial\mathcal{D})$ for $\alpha = 1, \ldots, \bar{\alpha}$, satisfying the compatibility condition

$$\int_{\partial\mathcal{D}} g_\alpha = 0, \tag{2}$$

the potential $U_\alpha^\star \in H^1_\diamond(\mathcal{D})$ is the solution to

$$-\operatorname{div}(\sigma^\star \nabla U_\alpha^\star) = 0 \text{ in } \mathcal{D}, \tag{3}$$
$$\sigma^\star \partial_\nu U_\alpha^\star = g_\alpha \text{ on } \partial\mathcal{D}, \tag{4}$$

where $\partial_\nu U_\alpha^\star := \nabla U_\alpha^\star \cdot \nu$, ν is the outward unit normal vector to $\mathcal{D}$ on $\partial\mathcal{D}$ and $H^1_\diamond(\mathcal{D})$ denotes the space of H^1-functions with vanishing integral mean on $\mathcal{D}$, i.e.,

$$H^1_\diamond(\mathcal{D}) := \left\{ W \in H^1(\mathcal{D}) : \int_{\mathcal{D}} W = 0 \right\}.$$

The variational formulation corresponding to the strong formulation (3),(4) reads: Find $U_\alpha^\star \in H^1_\diamond(\mathcal{D})$ such that

$$\int_{\mathcal{D}} \sigma^\star \nabla U_\alpha^\star \cdot \nabla W = \int_{\partial\mathcal{D}} g_\alpha W, \qquad \forall\, W \in H^1(\mathcal{D}). \tag{5}$$

The EIT problem consists in reconstructing the ground truth $\sigma^\star$ from the knowledge of a data set $\{g_\alpha, h_\alpha\}_{\alpha=1}^{\bar{\alpha}}$, where $h_\alpha := U_\alpha^\star|_{\partial\mathcal{D}} + \eta_\alpha$ are noisy boundary measurements of the potentials $U_\alpha^\star$, and $\eta_\alpha \in L^2(\partial\mathcal{D})$ is a measurement noise. A possible approach to compute a numerical approximation of the ground truth is to minimize the least-squares misfit

$$\sum_{\alpha=1}^{\bar{\alpha}} \int_{\partial\mathcal{D}} (U_\alpha(\sigma) - h_\alpha)^2,$$

where the model $U_\alpha(\sigma)$ satisfies the same PDE as (3),(4), but with the trial conductivity σ instead of the ground truth $\sigma^\star$. Another popular approach, employed in the present paper, is to consider the so-called Kohn-Vogelius functional [33]. We actually employ a variation, based on mixed boundary conditions, of the Kohn-Vogelius approach, following [38]. For $\alpha = 1, \ldots, \bar{\alpha}$, introduce $U_\alpha \in H^1_{a,h_\alpha}(\mathcal{D})$ and $V_\alpha \in H^1_{b,h_\alpha}(\mathcal{D})$ solutions of

$$\int_{\mathcal{D}} \sigma \nabla U_\alpha \cdot \nabla W = \int_{\Gamma_b} g_\alpha W \quad \text{for all } W \in H^1_{a,0}(\mathcal{D}), \tag{6}$$
$$\int_{\mathcal{D}} \sigma \nabla V_\alpha \cdot \nabla W = \int_{\Gamma_a} g_\alpha W \quad \text{for all } W \in H^1_{b,0}(\mathcal{D}), \tag{7}$$

with $\overline{\Gamma_a} \cup \overline{\Gamma_b} = \partial\mathcal{D}$, $\Gamma_a \neq \emptyset$, $\Gamma_b \neq \emptyset$, $g_\alpha \in L^2(\partial\mathcal{D})$, $h_\alpha \in H^{1/2}(\partial\mathcal{D})$ and

$$H^1_{a,h_\alpha}(\mathcal{D}) := \{W \in H^1(\mathcal{D}) \mid W = h_\alpha \text{ on } \Gamma_a\},$$
$$H^1_{b,h_\alpha}(\mathcal{D}) := \{W \in H^1(\mathcal{D}) \mid W = h_\alpha \text{ on } \Gamma_b\}.$$

When σ is sufficiently smooth, the strong formulations corresponding to (6) and (7) are

$$-\operatorname{div}(\sigma \nabla U_\alpha) = 0 \text{ in } \mathcal{D}, \tag{8}$$
$$\sigma \partial_\nu U_\alpha = g_\alpha \text{ on } \Gamma_b, \tag{9}$$
$$U_\alpha = h_\alpha \text{ on } \Gamma_a \tag{10}$$

and

$$-\operatorname{div}(\sigma\nabla V_\alpha) = 0 \text{ in } \mathcal{D}, \tag{11}$$

$$\sigma\partial_\nu V_\alpha = g_\alpha \text{ on } \Gamma_a, \tag{12}$$

$$V_\alpha = h_\alpha \text{ on } \Gamma_b, \tag{13}$$

respectively. When σ is piecewise constant, strong formulations can also be written using transmission conditions.

An approximation of the ground truth $\sigma^\star$ is obtained by minimizing the Kohn-Vogelius cost functional

$$J(\sigma) := \frac{1}{2}\sum_{\alpha=1}^{\bar\alpha}\zeta_\alpha\int_{\mathcal{D}}(U_\alpha(\sigma)-V_\alpha(\sigma))^2 \tag{14}$$

with respect to $\sigma \in L^\infty(\mathcal{D})$. The weights ζ_α are used for numerical purposes to balance the terms in the sum, so that they have a comparable magnitude; see Section 6 for more details.

We briefly explain in which sense this provides an approximation of the ground truth $\sigma^\star$. In the noiseless case $\eta_\alpha = 0$, $\alpha = 1,\dots,\bar\alpha$, we have $h_\alpha := U_\alpha^\star|_{\partial\mathcal{D}}$ and writing the equation for $U_\alpha(\sigma^\star) - U_\alpha^\star$ using (5) and (6) we get

$$\int_{\mathcal{D}}\sigma^\star\nabla(U_\alpha(\sigma^\star)-U_\alpha^\star)\cdot\nabla W = -\int_{\partial\mathcal{D}} g_\alpha W + \int_{\Gamma_b} g_\alpha W = \int_{\Gamma_a} g_\alpha W = 0 \quad \text{for all } W \in H^1_{a,0}(\mathcal{D}),$$
$$U_\alpha(\sigma^\star) - U_\alpha^\star = 0 \text{ on } \Gamma_a,$$

hence $U_\alpha(\sigma^\star) \equiv U_\alpha^\star$ in $\mathcal{D}$, and in a similar way $V_\alpha(\sigma^\star) \equiv U_\alpha^\star$ in $\mathcal{D}$. Thus, we get

$$0 = J(\sigma^\star) = \min_{\sigma\in L^\infty(\mathcal{D})} J(\sigma),$$

and $\sigma^\star$ is indeed a global minimizer of J. Conversely, if $\hat\sigma$ also satisfies $0 = J(\hat\sigma)$, we then have $U_\alpha(\hat\sigma) = V_\alpha(\hat\sigma)$ almost everywhere in $\mathcal{D}$, $\alpha = 1,\dots,\bar\alpha$, hence $\hat\sigma\partial_\nu U_\alpha(\hat\sigma) = g_\alpha$ on $\partial\mathcal{D}$, $U_\alpha(\hat\sigma) = h_\alpha$ on $\partial\mathcal{D}$, thus $\hat\sigma$ is also a solution of the inverse problem. The additional property $\hat\sigma = \sigma^\star$ depends on the uniqueness of the solution of the inverse problem for the considered class of σ, which is independent of the optimization approach employed to solve the inverse problem. This shows that minimizing the Kohn-Vogelius functional is a meaningful approach for approximating the solution of the inverse problem, also in the presence of noise if the problem is sufficiently stable.

Since EIT is a severely ill-posed inverse problem, it is useful to include prior knowledge on the ground truth $\sigma^\star$ in the mathematical model in order to reduce the ill-posedness. In this work we consider such a specific configuration where $\sigma^\star$ is piecewise constant. To make this statement precise, let us introduce partitions of $\mathcal{D}_0 \subset \mathcal{D}$, called *diagrams*, indexed by a set $\mathcal{K}$ of indices.

Definition 1 ($\mathcal{K}$-diagrams of $\mathcal{D}_0$)**.** *Let $\mathbb{P}$ denote the set of open subsets of $\mathcal{D}_0$, with $\mathcal{D}_0 \subset \mathcal{D} \subset \mathbb{R}^2$. For a given finite set of indices $\mathcal{K} \subset \mathbb{N}^*$, $\mathbb{P}_\mathcal{K}(\mathcal{D}_0)$ denotes the set of so-called $\mathcal{K}$-diagrams $\mathbf{\Omega} := \{\Omega_k\}_{k\in\mathcal{K}}$ with respect to $\mathcal{D}_0$, with the phases $\Omega_k \in \mathbb{P}$ for all $k \in \mathcal{K}$, $\Omega_k \cap \Omega_\ell = \emptyset$ for all $\{k,\ell\} \subset \mathcal{K}$, $k \neq \ell$ and $\bigcup_{k\in\mathcal{K}}\overline{\Omega_k} = \overline{\mathcal{D}_0}$.*

Let $\mathcal{D}_0 \subset \mathcal{D}$, $\mathcal{K} \subset \mathbb{N}^*$ be given and $\mathbf{\Omega} := \{\Omega_k\}_{k\in\mathcal{K}}$ be a $\mathcal{K}$-diagram with respect to $\mathcal{D}_0$. Denoting by $\Omega_0 := \mathcal{D} \setminus \overline{\mathcal{D}_0}$, we assume that $\sigma = \sigma_{\mathbf{\Omega}}$ is piecewise constant and has the form

$$\sigma_{\mathbf{\Omega}} := \sigma_0\chi_{\Omega_0} + \sum_{i\in\mathcal{K}}\sigma_i\chi_{\Omega_i},$$

where χ_{Ω_i} denotes the characteristic function of Ω_i and σ_i are constants. In this work, we will assume that $\mathcal{K}$, σ_i, $\forall i \in \mathcal{K}$, Ω_0 and σ_0 are known for the sake of simplicity. Then the cost function (14) becomes

$$\mathfrak{J}(\mathbf{\Omega}) := J(\sigma_{\mathbf{\Omega}}) = \frac{1}{2}\sum_{\alpha=1}^{\bar\alpha}\zeta_\alpha\int_{\mathcal{D}}(U_\alpha(\sigma_{\mathbf{\Omega}})-V_\alpha(\sigma_{\mathbf{\Omega}}))^2. \tag{15}$$

The problem of minimizing $\mathfrak{J}(\mathbf{\Omega})$ with respect to $\mathbf{\Omega}$ is called a *multiphase shape optimization problem.*

Note that we have made a distinction between the subset Ω_0 and the phases $\Omega_k, k \in \mathcal{K}$ of $\mathcal{D}$. Indeed, in our framework, Ω_0 is a known fixed subset of $\mathcal{D}$, whereas the other phases are subject to optimization. This is useful for certain applications and slightly generalizes the framework considered in [14] since we can also choose $\mathcal{D}_0 = \mathcal{D}$. In the EIT problem, Ω_0 will be taken as a thin layer along the boundary $\partial\mathcal{D}$, as in Figure 1. Its purpose is to avoid shape differentiability issues related to the low regularity of the data on $\partial\mathcal{D}$. In the conductivity problem with internal measurements, we will take $\mathcal{D}_0 = \mathcal{D}$, i.e., $\Omega_0 = \emptyset$, see Section 5.

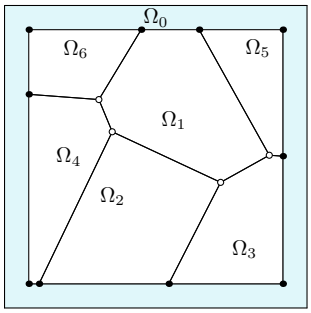

Figure 1: Illustration of the geometrical setting for the EIT problem. Here $\Omega_0 := \mathcal{D} \setminus \overline{\mathcal{D}_0}$ is a thin, fixed boundary layer, whereas the other phases $\Omega_k \subset \mathcal{D}, k \in \mathcal{K}$, form a Voronoi diagram and are subject to optimization. For future reference, the interior vertices (with respect to $\mathcal{D}_0$) are colored white (or empty) and the boundary vertices (with respect to $\mathcal{D}_0$) are colored black.

We will also consider the particular case where $\mathbf{\Omega}$ is a Voronoi diagram, as in [14]. Let $\mathcal{K}_{\text{vor}} = \{1, \dots, \kappa_0\}$ be a set of indices, $\mathbf{a} = \{a_k\}_{k\in\mathcal{K}_{\text{vor}}}$ be a set of points in the plane, the so-called *sites*, and let $\mathbf{\Omega}(\mathbf{a}) := \{\Omega_k(\mathbf{a})\}_{k\in\mathcal{K}_{\text{vor}}}$ be the Voronoi diagram associated with $\mathbf{a}$, where the cells of the diagram are defined by

$$\Omega_i(\mathbf{a}) := \{x \in \mathcal{D}_0 \text{ such that } \|x - a_i\| \leq \|x - a_j\| \text{ for all } j \in \mathcal{K}_{\text{vor}} \setminus \{i\}\}.$$

We also assume that the ground truth originates from a Voronoi diagram with the same conductivities σ_i, i.e.,

$$\sigma^\star = \sigma_0 \chi_{\Omega_0} + \sum_{i\in\mathcal{K}_{\text{vor}}} \sigma_i \chi_{\Omega_i(\mathbf{a}^\star)}.$$

Introducing the reduced cost function

$$G(\mathbf{a}) := \mathfrak{J}(\mathbf{\Omega}(\mathbf{a})), \tag{16}$$

we have reformulated the problem into the finite-dimensional optimization problem

$$\underset{\mathbf{a}\in\mathbb{R}^{2\kappa_0}}{\text{Minimize}}\, G(\mathbf{a}). \tag{17}$$

3 Sensitivity analysis for Voronoi diagrams

We provide general formulas for computing the gradient of cost functions depending on Voronoi diagrams, combining the theory of multiphase, non-smooth shape calculus [11, 36] and the theory developed in [13] for the sensitivity analysis with respect to minimization diagrams. The notion of distributed shape derivative [36, 38] and the regularity of solutions to the PDE play a key role in the existence of the gradient of the cost function, see Theorem 2. This section is similar to [14, Section 3], except that most definitions and results need to be adapted to account for the subset $\mathcal{D}_0$.

3.1 Multiphase shape optimization

Recall that $\mathcal{D}_0$ and $\mathcal{D}$, $\mathcal{D}_0 \subset \mathcal{D}$, are both bounded, Lipschitz, simply connected, and piecewise $\mathcal{C}^1$ domains. Denote by $\mathcal{S}$ and $\mathcal{S}_0$ the sets of singular points of $\partial\mathcal{D}$ and $\partial\mathcal{D}_0$, respectively, then the outward

unit normal vector ν to $\mathcal{D}$ is well-defined on $\partial\mathcal{D} \setminus \mathcal{S}$. For $r \geq 1$ and $0 \leq \beta \leq 1$, introduce

$$\mathcal{C}^{r,\beta}_{\partial\mathcal{D}}(\overline{\mathcal{D}}, \mathbb{R}^2) := \{\theta \in \mathcal{C}^{r,\beta}(\overline{\mathcal{D}}, \mathbb{R}^2) : \ \theta \cdot \nu = 0 \text{ on } \partial\mathcal{D} \setminus \mathcal{S} \text{ and } \theta = 0 \text{ on } \mathcal{S}\}, \tag{18}$$

$$\mathcal{C}^{r,\beta}_{c}(\overline{\mathcal{D}}, \mathbb{R}^2) := \{\theta \in \mathcal{C}^{r,\beta}(\overline{\mathcal{D}}, \mathbb{R}^2) : \ \theta \text{ has compact support in } \mathcal{D}\}, \tag{19}$$

$$\mathcal{C}^{r,\beta}_{c,\partial\mathcal{D}_0}(\overline{\mathcal{D}}, \mathbb{R}^2) := \{\theta \in \mathcal{C}^{r,\beta}_{c}(\overline{\mathcal{D}}, \mathbb{R}^2) : \ \theta \cdot \nu = 0 \text{ on } \partial\mathcal{D}_0 \setminus \mathcal{S}_0 \text{ and } \theta = 0 \text{ on } \mathcal{S}_0\}. \tag{20}$$

For the shape sensitivity analysis we will consider the following type of mappings.

Assumption 1. *Let $T : \overline{\mathcal{D}} \times [0, t_0] \to \overline{\mathcal{D}}$ be such that $T(\cdot, t) : \overline{\mathcal{D}} \to \overline{\mathcal{D}}$ is a bi-Lipschitz mapping for all $t \in [0, t_0]$, $t \mapsto T(\cdot, t) \in \mathcal{C}^1([0, t_0], \mathcal{C}^{0,1}(\overline{\mathcal{D}}, \mathbb{R}^2))$, $T(\cdot, 0)$ is the identity mapping, $T(\overline{\mathcal{D}}, t) = \overline{\mathcal{D}}$ and $T(\overline{\mathcal{D}_0}, t) = \overline{\mathcal{D}_0}$ for all $t \in [0, t_0]$.*

Let T be a mapping satisfying Assumption 1, then $T(\cdot, t) : \overline{\mathcal{D}} \to \overline{\mathcal{D}}$ maps interior points onto interior points and boundary points onto boundary points; see [19, Chapter 4, Section 5.1 and Remark 5.2]. Introducing $\theta := \partial_t T(\cdot, 0)$, we get $\theta \in \mathcal{C}^{0,1}_{\partial\mathcal{D}}(\overline{\mathcal{D}}, \mathbb{R}^2)$. Conversely, given $\theta \in \mathcal{C}^{0,1}_{\partial\mathcal{D}}(\overline{\mathcal{D}}, \mathbb{R}^2)$, there exists a mapping T satisfying Assumption 1 with $\theta = \partial_t T(\cdot, 0)$. For this purpose one can use for instance the velocity method [19, 45]. In what follows, if θ is given first, it will be implicit that T is the associated mapping satisfying Assumption 1.

For $\Omega \in \mathbb{P}$, introduce the family of perturbed domains

$$\Omega_t := T(\Omega, t). \tag{21}$$

For a set of indices $\mathcal{K} = \{1, \dots, \kappa\}$ and $\mathbf{\Omega} \in \mathbb{P}_{\mathcal{K}}(\mathcal{D}_0)$, see Definition 1, we define

$$\mathbf{\Omega}_t := T(\mathbf{\Omega}, t) := \{T(\Omega_k, t)\}_{k \in \mathcal{K}}. \tag{22}$$

Note that $\mathbf{\Omega}_t$ is also a $\mathcal{K}$-diagram of $\mathcal{D}_0$ for all $t \in [0, t_0]$. We now provide the definition of shape derivatives in the context of multiphase problems.

Definition 2 (Shape derivative)**.** *Let $\mathcal{J} : \mathbb{P}_{\mathcal{K}}(\mathcal{D}_0) \to \mathbb{R}$ be a multiphase shape functional, with $r \geq 1$ and $0 \leq \beta \leq 1$ or $(r, \beta) = (0, 1)$.*

(i) The Eulerian semiderivative of $\mathcal{J}$ at $\mathbf{\Omega} \in \mathbb{P}_{\mathcal{K}}(\mathcal{D}_0)$ in direction $\theta \in \mathcal{C}^{r,\beta}_{\partial\mathcal{D}}(\overline{\mathcal{D}}, \mathbb{R}^2)$ is defined by, when the limit exists,

$$d\mathcal{J}(\mathbf{\Omega})(\theta) := \lim_{t \searrow 0} \frac{\mathcal{J}(\mathbf{\Omega}_t) - \mathcal{J}(\mathbf{\Omega})}{t}. \tag{23}$$

(ii) $\mathcal{J}$ is said to be shape differentiable at $\mathbf{\Omega} \in \mathbb{P}_{\mathcal{K}}(\mathcal{D}_0)$ if it has an Eulerian semiderivative at $\mathbf{\Omega}$ for all $\theta \in \mathcal{C}^{r,\beta}_{\partial\mathcal{D}}(\overline{\mathcal{D}}, \mathbb{R}^2)$ and the mapping

$$d\mathcal{J}(\mathbf{\Omega})(\theta) : \mathcal{C}^{r,\beta}_{\partial\mathcal{D}}(\overline{\mathcal{D}}, \mathbb{R}^2) \to \mathbb{R}, \ \theta \mapsto d\mathcal{J}(\mathbf{\Omega})(\theta)$$

is linear and continuous, in which case $d\mathcal{J}(\mathbf{\Omega})(\theta)$ is called the shape derivative of $\mathcal{J}$ at $\mathbf{\Omega}$ in direction $\theta \in \mathcal{C}^{r,\beta}_{\partial\mathcal{D}}(\overline{\mathcal{D}}, \mathbb{R}^2)$.

Shape derivatives $d\mathcal{J}(\mathbf{\Omega})(\theta)$ can usually be written either as a sum of integrals on the edges of the diagram, called Hadamard form of the shape derivative or boundary expression, or as integrals on the phases Ω_k, $k \in \mathcal{K}_{\text{vor}}$, of the diagram, called distributed shape derivative, see [30, 36, 38, 48]. We recall the notion of tensor representation [36, 38], adapted to the context of multiphase problems, as in [14].

Definition 3 (Tensor representation of distributed shape derivative)**.** *Let $\mathbf{\Omega} \in \mathbb{P}_{\mathcal{K}}(\mathcal{D}_0)$ and assume $\mathcal{J} : \mathbb{P}_{\mathcal{K}}(\mathcal{D}_0) \mapsto \mathbb{R}$ has a shape derivative at $\mathbf{\Omega}$ in direction $\theta \in \mathcal{C}^{0,1}_{\partial\mathcal{D}}(\overline{\mathcal{D}}, \mathbb{R}^2)$. The shape derivative $d\mathcal{J}(\mathbf{\Omega})(\theta)$ admits a first-order tensor representation if there exist a first-order tensor $S_0(\mathbf{\Omega}) \in L^1(\mathcal{D}, \mathbb{R}^2)$ and a second order tensor $S_1(\mathbf{\Omega}) \in L^1(\mathcal{D}, \mathbb{R}^{2\times 2})$ such that*

$$d\mathcal{J}(\mathbf{\Omega})(\theta) = \int_{\mathcal{D}} S_1(\mathbf{\Omega}) : D\theta + S_0(\mathbf{\Omega}) \cdot \theta. \tag{24}$$

Remark 1. *Definitions 2 and 3 are formulated for θ in $\mathcal{C}^{r,\beta}_{\partial\mathcal{D}}(\overline{\mathcal{D}}, \mathbb{R}^2)$. Depending on the needs, we will often use θ in the smaller spaces $\mathcal{C}^{r,\beta}_{c}(\overline{\mathcal{D}}, \mathbb{R}^2)$ or $\mathcal{C}^{r,\beta}_{c,\partial\mathcal{D}_0}(\overline{\mathcal{D}}, \mathbb{R}^2)$, for which Definitions 2 and 3 also apply due to $\mathcal{C}^{r,\beta}_{c,\partial\mathcal{D}_0}(\overline{\mathcal{D}}, \mathbb{R}^2) \subset \mathcal{C}^{r,\beta}_{c}(\overline{\mathcal{D}}, \mathbb{R}^2) \subset \mathcal{C}^{r,\beta}_{\partial\mathcal{D}}(\overline{\mathcal{D}}, \mathbb{R}^2)$.*

3.2 Derivative with respect to the Voronoi sites

We compute the gradient with respect to $\mathbf{a}$ of a general function

$$\mathcal{G}(\mathbf{a}) := \mathcal{J}(\mathbf{\Omega}(\mathbf{a})), \tag{25}$$

where $\mathcal{J} : \mathbb{P}_{\mathcal{K}_{\rm vor}}(\mathcal{D}_0) \to \mathbb{R}$ is a multiphase shape functional and $\mathbf{\Omega}(\mathbf{a})$ is a Voronoi diagram, in the case where the shape derivative $d\mathcal{J}(\mathbf{\Omega}(\mathbf{a}))(\theta)$ admits the first-order tensor representation (24). As $\mathcal{G}(\mathbf{a})$ is the composition of $\mathbf{a} \mapsto \mathbf{\Omega}(\mathbf{a})$ with a shape functional $\mathbf{\Omega} \mapsto \mathcal{J}(\mathbf{\Omega})$, the derivative of $\mathcal{G}(\mathbf{a})$ is obtained via a sort of chain rule; see [13, 14].

In this section and in the rest of the paper we assume in addition that $\mathcal{D}$ and $\mathcal{D}_0$ are defined as

$$\mathcal{D} := \{x \in \mathbb{R}^2 : \ \varphi(x) < \delta\}, \qquad \mathcal{D}_0 := \{x \in \mathbb{R}^2 : \ \varphi(x) < 0\} \tag{26}$$

with $\delta \geq 0$, $\varphi(x) := \min_{\ell \in \mathcal{K}_\mathcal{D}} \varphi_\ell(x)$ and $\varphi_\ell \in \mathcal{C}^\infty(\mathbb{R}^2, \mathbb{R})$ for all $\ell \in \mathcal{K}_\mathcal{D} := \{\kappa_0 + 1, \dots, \kappa_0 + \kappa_1\}$. Note that $\mathcal{D}_0 = \mathcal{D}$ if $\delta = 0$. In the EIT case we take $\delta > 0$ and introduce the intermediate set

$$\mathcal{D}_{\hat\delta} := \{x \in \mathbb{R}^2 : \ \varphi(x) < \hat\delta\}, \tag{27}$$

where $\hat\delta$ satisfies $0 < \hat\delta < \delta$, so that $\mathcal{D}_0 \subsetneq \mathcal{D}_{\hat\delta} \subsetneq \mathcal{D}$.

For $\ell \in \mathcal{K}_\mathcal{D}$, introduce $\partial_\ell \mathcal{D}_0 := \{x \in \partial\mathcal{D}_0 : \ \varphi_\ell(x) = 0\}$, then $\partial\mathcal{D}_0 = \cup_{\ell \in \mathcal{K}_\mathcal{D}} \partial_\ell \mathcal{D}_0$. For $\{i, j, k\} \subset \mathcal{K}_{\rm vor}$ and $\ell \in \mathcal{K}_\mathcal{D}$, define $Y_{ijk}(t) := \overline{\Omega_i(\mathbf{a} + t\delta\mathbf{a})} \cap \overline{\Omega_j(\mathbf{a} + t\delta\mathbf{a})} \cap \overline{\Omega_k(\mathbf{a} + t\delta\mathbf{a})}$ and $X_{ij\ell}(t) := \overline{\Omega_i(\mathbf{a} + t\delta\mathbf{a})} \cap \overline{\Omega_j(\mathbf{a} + t\delta\mathbf{a})} \cap \partial_\ell\mathcal{D}_0$. The set $Y_{ijk}(t)$ is a set of *interior vertices* (with respect to $\mathcal{D}_0$), i.e., points in $\mathcal{D}_0$ at the intersection of three cells. The set $X_{ij\ell}(t)$ is a set of *boundary vertices* (with respect to $\mathcal{D}_0$), i.e., points on $\partial\mathcal{D}_0$ at the intersection of two cells; see Figure 1. We will write $Y_{ijk} := Y_{ijk}(0)$ and $X_{ij\ell} := X_{ij\ell}(0)$ for simplicity. The set Y_{ijk} contains at most one point, whereas $X_{ij\ell}$ may contain several points. For $k \in \mathcal{K}_{\rm vor} \setminus \{i\}$ and $\ell \in \mathcal{K}_\mathcal{D}$, $E_{ik}(\mathbf{a} + t\delta\mathbf{a}) := \overline{\Omega_i(\mathbf{a} + t\delta\mathbf{a})} \cap \overline{\Omega_k(\mathbf{a} + t\delta\mathbf{a})}$ denotes an *interior edge* of the diagram $\mathbf{\Omega}(\mathbf{a} + t\delta\mathbf{a})$, while $E_{i\ell}(\mathbf{a} + t\delta\mathbf{a}) := \overline{\Omega_i(\mathbf{a} + t\delta\mathbf{a})} \cap \partial_\ell\mathcal{D}_0$ denotes a *boundary edge* of the diagram (with respect to $\mathcal{D}_0$). We denote by $\mathcal{E}_i^{\rm int}$ the set of interior edges of the cell $\Omega_i(\mathbf{a})$ with respect to $\mathcal{D}_0$, i.e., edges that are included in $\mathcal{D}_0$.

We now provide a set of geometric assumptions required to avoid degenerate cases and perform the sensitivity analysis of Voronoi diagrams; see Example 1 and Figure 2 in Section 4.2 for an example of degenerate case. We refer to [13, Section 4] and [14, Section 3.2] for detailed explanations.

Assumption 2. *Suppose that:*

- *(Non-degeneracy of interfaces) There holds $\|\nabla_x \varphi_\ell(x)\| > 0$ for all $x \in \partial_\ell\mathcal{D}$ and for all $\ell \in \mathcal{K}_\mathcal{D}$, and $\|a_i - a_j\| > 0$ for all $\{i, j\} \subset \mathcal{K}_{vor}$.*
- *(Non-degeneracy of vertices) For all $\{i, j, k\} \subset \mathcal{K}_{vor}$ such that $Y_{ijk} \neq \emptyset$ we have $(a_j - a_i)^\perp \cdot (a_k - a_i) \neq 0$ and $Y_{ijk} \notin \overline{V_m(\mathbf{a})}$, for all $m \in \mathcal{K}_{vor} \setminus \{i, j, k\}$. In addition, for all $\{i, j\} \subset \mathcal{K}_{vor}$ and $\ell \in \mathcal{K}_\mathcal{D}$ and all $v \in X_{ij\ell}$ we have $(a_j - a_i)^\perp \cdot \nabla\varphi_\ell(v) \neq 0$, $v \notin \overline{V_m(\mathbf{a})}$, for all $m \in \mathcal{K}_{vor} \setminus \{i, j\}$, and $v \notin \mathcal{T}_{\partial\mathcal{D}_0}$, where $\mathcal{T}_{\partial\mathcal{D}_0}$ is the finite set of corners of $\mathcal{D}_0$.*[1]

Under Assumption 2, the cell $\Omega_i(\mathbf{a} + t\delta\mathbf{a})$ can be parameterized by a bi-Lipschitz mapping $T(\cdot, t)$ satisfying Assumption 1, such that its derivative $\theta := \partial_t T(\cdot, 0)$ is described explicitly as a function of the sites $\mathbf{a}$. This parameterization is described in the following theorem, which is a particular case of [13, Theorem 5], slightly adapted to our situation where $\Omega_0 = \mathcal{D} \setminus \overline{\mathcal{D}_0}$ is fixed.

Theorem 1. *Suppose Assumption 2 holds. Then there exist $t_0 > 0$ and a mapping $T : \overline{\mathcal{D}} \times [0, t_0] \to \mathbb{R}^2$ with the following properties. For each $i \in \mathcal{K}_{vor}$ we have $T(\Omega_i(\mathbf{a}), t) = \Omega_i(\mathbf{a} + t\delta\mathbf{a})$, $T(E_{ik}(\mathbf{a}), t) = E_{ik}(\mathbf{a} + t\delta\mathbf{a})$ for all $k \in \mathcal{K}_{vor} \setminus \{i\}$, $T(E_{i\ell}(\mathbf{a}), t) = E_{i\ell}(\mathbf{a} + t\delta\mathbf{a})$ for all $\ell \in \mathcal{K}_\mathcal{D}$, $T(\partial\Omega_i(\mathbf{a}), t) = \partial\Omega_i(\mathbf{a} + t\delta\mathbf{a})$ and $T(\cdot, t) : \overline{\Omega_i(\mathbf{a})} \to \overline{\Omega_i(\mathbf{a} + t\delta\mathbf{a})}$ is bi-Lipschitz for all $t \in [0, t_0]$. Also, for all $t \in [0, t_0]$ we have*

[1] This corrects [14, Assumption 1], where the conditions "$Y_{ijk} \notin \overline{V_m(\mathbf{a})}$, for all $m \in \mathcal{K}_{\rm vor} \setminus \{i, j, k\}$" and "$v \notin \overline{V_m(\mathbf{a})}$, for all $m \in \mathcal{K}_{\rm vor} \setminus \{i, j\}$, and $v \notin \mathcal{T}_{\partial\mathcal{D}_0}$" were missing. These conditions are necessary to avoid degenerate cases such as the one presented in Figure 2, where four cells have a non-empty intersection.

$T(\Omega_0,t)=\Omega_0$, $T(\partial\Omega_0,t)=\partial\Omega_0$ and $T(\cdot,t):\overline{\Omega_0}\to\overline{\Omega_0}$ is bi-Lipschitz. In addition, $t\mapsto T(\cdot,t)$ is differentiable at $t=0$, $\theta:=\partial_t T(\cdot,0)$ satisfies $\theta\in\mathcal{C}^{0,1}_{c,\partial\mathcal{D}_0}(\overline{\mathcal{D}},\mathbb{R}^2)$ and

$$\theta(x)\cdot\nu(x)=\frac{\nabla_a\phi(x,a_k)\cdot\delta a_k-\nabla_a\phi(x,a_i)\cdot\delta a_i}{\|\nabla_x\phi(x,a_k)-\nabla_x\phi(x,a_i)\|}\ \text{for all } x\in E_{ik}(\mathbf{a}) \text{ and all } k\in\mathcal{K}_{vor}\setminus\{i\},\tag{28}$$

$$\theta(x)\cdot\nu(x)=0 \text{ for all } x\in E_{i\ell}(\mathbf{a}) \text{ for all } \ell\in\mathcal{K}_{\mathcal{D}},\tag{29}$$

$$\theta(x)\cdot\nu(x)=0 \text{ for all } x\in\partial\Omega_0,\tag{30}$$

where ν is the outward unit normal vector to $\Omega_i(\mathbf{a})$ or Ω_0, and $\phi(x,a):=\|x-a\|^2$.

Remark 2. *Note that $\|\nabla_x\phi(x,a_k)-\nabla_x\phi(x,a_i)\|=2\|a_k-a_i\|$ and Assumption 2 implies $\|a_k-a_i\|>0$, so that (28) is well-defined.*

Equation (30) expresses the fact that the boundary of Ω_0 is not moving. In the case $\mathcal{D}_0\subsetneq\mathcal{D}$, property (29) is contained in (30), but if $\mathcal{D}_0=\mathcal{D}$ then (30) is void and (29) is the relevant property. Now introduce $\mathbf{\Omega}(\mathbf{a}+t\delta\mathbf{a}):=\{\Omega_k(\mathbf{a}+t\delta\mathbf{a})\}_{k\in\mathcal{K}_{\rm vor}}$ and $\mathcal{G}(\mathbf{a}+t\delta\mathbf{a}):=\mathcal{J}(\mathbf{\Omega}(\mathbf{a}+t\delta\mathbf{a}))$. By definition of the Voronoi diagram, we have $\mathbf{\Omega}(\mathbf{a}+t\delta\mathbf{a})\in\mathbb{P}_{\mathcal{K}_{\rm vor}}(\mathcal{D}_0)$ for all $t\in[0,t_0]$. In view of Theorem 1 we have $\mathbf{\Omega}(\mathbf{a}+t\delta\mathbf{a})=T(\mathbf{\Omega}(\mathbf{a}),t)=\{T(\Omega_k(\mathbf{a}),t)\}_{k\in\mathcal{K}_{\rm vor}}$. Recall that $\mathcal{E}_i^{\rm int}$ is the set of interior edges of the cell $\Omega_i(\mathbf{a})$, i.e., edges that are included in $\mathcal{D}_0$. We have the following result in the case $\delta>0$.

Theorem 2. *Suppose Assumption 2 holds, that $\mathcal{J}:\mathbb{P}_{\mathcal{K}_{vor}}(\mathcal{D}_0)\to\mathbb{R}$ is shape differentiable at $\mathbf{\Omega}(\mathbf{a})$ and that the shape derivative $d\mathcal{J}(\mathbf{\Omega}(\mathbf{a}))(\theta)$ admits the first-order tensor representation (24) for all $\theta\in\mathcal{C}^{0,1}_{c,\partial\mathcal{D}_0}(\overline{\mathcal{D}},\mathbb{R}^2)$. Assume further that $S_1(\mathbf{\Omega}(\mathbf{a}))|_{\Omega_i(\mathbf{a})}\in W^{1,1}(\Omega_i(\mathbf{a}),\mathbb{R}^{2\times2})$ for all $i\in\mathcal{K}_{vor}$ and that $S_1(\mathbf{\Omega}(\mathbf{a}))|_{\Omega_0\cap\mathcal{D}_{\hat\delta}}\in W^{1,1}(\Omega_0\cap\mathcal{D}_{\hat\delta},\mathbb{R}^2)$ for all $0<\hat\delta<\delta$, where $\mathcal{D}_{\hat\delta}$ is defined in (27). Then the gradient of $\mathcal{G}(\mathbf{a})$, defined in (25), is given by*

$$\nabla\mathcal{G}(\mathbf{a})\cdot\delta\mathbf{a}=\sum_{i\in\mathcal{K}_{vor}}\sum_{E\in\mathcal{E}_i^{\rm int}}\int_E(S_1(\mathbf{\Omega}(\mathbf{a}))\nu\cdot\nu)|_{\partial\Omega_i(\mathbf{a})}\frac{(x-a_i)\cdot\delta a_i-(x-a_{k(i,E)})\cdot\delta a_{k(i,E)}}{\|a_{k(i,E)}-a_i\|}dx,\tag{31}$$

where $k(i,E)$ is the index such that $E=\overline{\Omega_i(\mathbf{a})}\cap\overline{\Omega_{k(i,E)}(\mathbf{a})}$.

Proof. In this proof, we write $\mathbf{\Omega}$ instead of $\mathbf{\Omega}(\mathbf{a})$ for simplicity. Since $d\mathcal{J}(\mathbf{\Omega})(\theta)$ admits the first-order tensor representation (24) for all $\theta\in\mathcal{C}^{0,1}_{c,\partial\mathcal{D}_0}(\overline{\mathcal{D}},\mathbb{R}^2)$, $\Omega_i(\mathbf{a})$ is Lipschitz, and using the regularity assumptions on $S_1(\mathbf{\Omega})$, one can prove that $\mathrm{div}(S_1(\mathbf{\Omega}))=S_0(\mathbf{\Omega})$ in $\Omega_0\cap\mathrm{supp}(\theta)$, by taking $\hat\delta$ sufficiently close to δ, and also in $\Omega_i(\mathbf{a})$ for all $i\in\mathcal{K}_{\rm vor}$, using [36, Proposition 1]. Then we can apply the divergence theorem in each $\Omega_i(\mathbf{a})$ and in Ω_0, which yields, using $\mathrm{div}(S_1(\mathbf{\Omega}))=S_0(\mathbf{\Omega})$,

$$\begin{aligned}
d\mathcal{J}(\mathbf{\Omega})(\theta)&=\int_{\mathcal{D}}S_1(\mathbf{\Omega}):D\theta+S_0(\mathbf{\Omega})\cdot\theta\,dx\\
&=\int_{\Omega_0}S_1(\mathbf{\Omega}):D\theta+S_0(\mathbf{\Omega})\cdot\theta\,dx+\sum_{i\in\mathcal{K}_{\rm vor}}\int_{\Omega_i(\mathbf{a})}S_1(\mathbf{\Omega}):D\theta+S_0(\mathbf{\Omega})\cdot\theta\,dx\\
&=\int_{\Omega_0}\mathrm{div}(S_1(\mathbf{\Omega})^{\mathsf T}\theta)\,dx+\sum_{i\in\mathcal{K}_{\rm vor}}\int_{\Omega_i(\mathbf{a})}\mathrm{div}(S_1(\mathbf{\Omega})^{\mathsf T}\theta)\,dx\\
&=\int_{\partial\Omega_0}S_1(\mathbf{\Omega})\nu\cdot\theta\,dx+\sum_{i\in\mathcal{K}_{\rm vor}}\int_{\partial\Omega_i(\mathbf{a})}S_1(\mathbf{\Omega})\nu\cdot\theta\,dx
\end{aligned}$$

and then

$$\begin{aligned}
d\mathcal{J}(\mathbf{\Omega})(\theta)=&\int_{\partial\Omega_0}(S_1(\mathbf{\Omega})\nu\cdot\nu)\theta\cdot\nu\,dx+\sum_{i\in\mathcal{K}_{\rm vor}}\int_{\partial\Omega_i(\mathbf{a})}(S_1(\mathbf{\Omega})\nu\cdot\nu)\theta\cdot\nu\,dx\\
&+\int_{\partial\Omega_0}(S_1(\mathbf{\Omega})\nu\cdot\tau)\theta\cdot\tau\,dx+\sum_{i\in\mathcal{K}_{\rm vor}}\int_{\partial\Omega_i(\mathbf{a})}(S_1(\mathbf{\Omega})\nu\cdot\tau)\theta\cdot\tau\,dx,
\end{aligned}\tag{32}$$

where τ denotes a unit tangent vector on $\partial\Omega_i(\mathbf{a})$ or $\partial\Omega_0$.

Now, let E be an edge of the diagram $\mathbf{\Omega}$; E can be an interior or boundary edge with respect to $\mathcal{D}_0$. Let $\hat{\theta} \in \mathcal{C}^{0,1}_{c,\partial\mathcal{D}_0}(\overline{\mathcal{D}}, \mathbb{R}^2)$ be a vector field such that $\hat{\theta} \cdot \nu = 0$ on E, $\hat{\theta}(v) = 0$ for all vertices v of E and the intersection of $\mathrm{supp}(\hat{\theta})$ with any other edge of the diagram $\mathbf{\Omega}$ is empty. Then the mapping $\hat{T}$ such that $\hat{T}(\cdot, t) = I_2 + t\hat{\theta}$ for all $t \in [0, t_0]$ satisfies Assumption 1 for sufficiently small t_0 and we have $\mathbf{\Omega}_t = \hat{T}(\mathbf{\Omega}, t) = \mathbf{\Omega}$ for all $t \in [0, t_0]$ in view of the properties of $\hat{\theta}$, hence $d\mathcal{J}(\mathbf{\Omega})(\hat{\theta}) = 0$. The edge E is either at the interface of exactly two cells, or at the interface of a cell and Ω_0. In any case, we can denote by $k_1(E)$ and $k_2(E)$ the indices of the neighboring sets of E. Thus, using (32) we have

$$\begin{aligned} 0 = d\mathcal{J}(\mathbf{\Omega})(\hat{\theta}) &= \int_{\partial\Omega_0} (S_1(\mathbf{\Omega})\nu \cdot \tau)\hat{\theta} \cdot \tau \, dx + \sum_{i \in \mathcal{K}_{\mathrm{vor}}} \int_{\partial\Omega_i(\mathbf{a})} (S_1(\mathbf{\Omega})\nu \cdot \tau)\hat{\theta} \cdot \tau \, dx \\ &= \int_E [\![S_1(\mathbf{\Omega})\nu \cdot \tau]\!]_E \hat{\theta} \cdot \tau, \end{aligned} \tag{33}$$

where the jump is defined as

$$[\![S_1(\mathbf{\Omega})\nu \cdot \tau]\!]_E := (S_1(\mathbf{\Omega})\nu \cdot \tau)|_{\partial\Omega_{k_1(E)}(\mathbf{a})} - (S_1(\mathbf{\Omega})\nu \cdot \tau)|_{\partial\Omega_{k_2(E)}(\mathbf{a})}.$$

Since (33) holds for any $\hat{\theta}$ with such properties, this shows that $[\![S_1(\mathbf{\Omega})\nu \cdot \tau]\!]_E = 0$, for all edges E of the diagram $\mathbf{\Omega}$. Thus, the tangential terms in (32) vanish and we obtain, for all $\theta \in \mathcal{C}^{0,1}_{c,\partial\mathcal{D}_0}(\overline{\mathcal{D}}, \mathbb{R}^2)$,

$$d\mathcal{J}(\mathbf{\Omega})(\theta) = \int_{\partial\Omega_0} (S_1(\mathbf{\Omega})\nu \cdot \nu)\theta \cdot \nu \, dx + \sum_{i \in \mathcal{K}_{\mathrm{vor}}} \int_{\partial\Omega_i(\mathbf{a})} (S_1(\mathbf{\Omega})\nu \cdot \nu)\theta \cdot \nu \, dx. \tag{34}$$

Now, let T be the mapping given in Theorem 1. Using Theorem 1 we have $\mathcal{G}(\mathbf{a} + t\delta\mathbf{a}) = \mathcal{J}(\mathbf{\Omega}(\mathbf{a} + t\delta\mathbf{a})) = \mathcal{J}(T(\mathbf{\Omega}, t))$. Setting $\theta := \partial_t T(\cdot, 0)$, we have $\theta \in \mathcal{C}^{0,1}_{c,\partial\mathcal{D}_0}(\overline{\mathcal{D}}, \mathbb{R}^2)$ according to Theorem 1, hence we obtain

$$\nabla\mathcal{G}(\mathbf{a}) \cdot \delta\mathbf{a} = \frac{d}{dt}(\mathcal{J}(\mathbf{\Omega}(\mathbf{a} + t\delta\mathbf{a})))|_{t=0} = d\mathcal{J}(\mathbf{\Omega})(\theta).$$

Using the fact that $\phi(x, a) = \|x - a\|^2$ we get $\nabla_a \phi(x, a_i) = -2(x - a_i)$ and, using (28),

$$\theta(x) \cdot \nu(x) = \frac{(x - a_i) \cdot \delta a_i - (x - a_{k(i,E)}) \cdot \delta a_{k(i,E)}}{\|a_{k(i,E)} - a_i\|} \text{ for all } x \in E_{ik}(\mathbf{a}).$$

Finally, using also (30) and (34) we obtain (31). □

Remark 3. *In the statement of Theorem 2, the assumption $S_1(\mathbf{\Omega}(\mathbf{a}))|_{\mathcal{D}_{\hat{\delta}}} \in W^{1,1}(\mathcal{D}_{\hat{\delta}}, \mathbb{R}^2)$ for all $0 < \hat{\delta} < \delta$ describes the fact that one only needs to prove higher regularity of $S_1(\mathbf{\Omega}(\mathbf{a}))$ away from the boundary of $\mathcal{D}$, as $\mathcal{D}_{\hat{\delta}} \subsetneq \mathcal{D}$. The assumption needs to be formulated that way as $S_1(\mathbf{\Omega}(\mathbf{a}))$ has a low regularity on $\partial\mathcal{D}$ in the EIT problem.*

The following result is an immediate consequence of Theorem 2; it is useful for the numerical implementation.

Corollary 1. *Under the assumptions of Theorem 2, we have*

$$\nabla\mathcal{G}(\mathbf{a}) \cdot \delta\mathbf{a} = \sum_{i \in \mathcal{K}_{vor}} \sum_{E \in \mathcal{E}_i^{\mathrm{int}}} \delta a_{k(i,E)} \cdot \lambda_{k,E} + \delta a_i \cdot \lambda_{i,E}, \tag{35}$$

with

$$\lambda_{k,E} = -\int_E (S_1(\mathbf{\Omega}(\mathbf{a}))\nu \cdot \nu) \frac{(x - a_{k(i,E)})}{\|a_{k(i,E)} - a_i\|} dx, \qquad \lambda_{i,E} = \int_E (S_1(\mathbf{\Omega}(\mathbf{a}))\nu \cdot \nu) \frac{(x - a_i)}{\|a_{k(i,E)} - a_i\|} dx.$$

4 Gradient of cost function for EIT

In this section, we consider the EIT problem. We take $\bar{\alpha} = 1$, $\zeta_1 = 1$, and we write U, V, g, h instead of U_1, V_1, g_1, h_1, to simplify the notation. The expression of the shape derivative in the case $\bar{\alpha} > 1$ and $\zeta_1 \neq 1$ can be obtained straightforwardly by summing over $\alpha = 1, \ldots, \bar{\alpha}$. We require the following assumption to prove shape differentiability.

Assumption 3. *Let $\mathcal{K} \subset \mathbb{N}^*$ and suppose $\mathbf{\Omega} \in \mathbb{P}_{\mathcal{K}}(\mathcal{D}_0)$, $h \in H^{1/2}(\partial\mathcal{D})$, $g \in L^2(\partial\mathcal{D})$.*

We now provide the shape derivative of the cost function $\mathfrak{J}(\mathbf{\Omega})$ for EIT, see definition (15). In this section we prove the shape differentiability in the general case of a $\mathcal{K}$-diagram $\mathbf{\Omega}$. The particular case of Voronoi diagrams is treated in the next sections. The Kohn-Vogelius approach with mixed boundary conditions, described in Section 2, is similar to the problems considered in [38], but we take a different approach to deal with the non-homogeneous Dirichlet conditions. Suppose Assumption 3 holds, then we introduce the function $\mathcal{H} \in H^1(\mathcal{D})$ solution to

$$\begin{aligned} -\Delta\mathcal{H} &= 0 \text{ in } \mathcal{D}, \\ \mathcal{H} &= h \text{ on } \partial\mathcal{D}, \end{aligned}$$

and $\bar{U} \in H^1_{a,0}(\mathcal{D})$, $\bar{V} \in H^1_{b,0}(\mathcal{D})$ solutions to

$$\int_{\mathcal{D}} \sigma_{\mathbf{\Omega}} \nabla\bar{U} \cdot \nabla W = -\int_{\mathcal{D}} \sigma_{\mathbf{\Omega}} \nabla\mathcal{H} \cdot \nabla W + \int_{\Gamma_b} gW \quad \text{for all } W \in H^1_{a,0}(\mathcal{D}), \tag{36}$$

$$\int_{\mathcal{D}} \sigma_{\mathbf{\Omega}} \nabla\bar{V} \cdot \nabla W = -\int_{\mathcal{D}} \sigma_{\mathbf{\Omega}} \nabla\mathcal{H} \cdot \nabla W + \int_{\Gamma_a} gW \quad \text{for all } W \in H^1_{b,0}(\mathcal{D}). \tag{37}$$

Thus we have $U = \bar{U} + \mathcal{H}$ and $V = \bar{V} + \mathcal{H}$. It is easier to work with $\bar{U}, \bar{V}$ instead of U, V, as they both satisfy homogeneous Dirichlet conditions on Γ_a and Γ_b, respectively.

Theorem 3 (distributed shape derivative)**.** *Suppose Assumption 3 holds, the mapping T satisfies Assumption 1 and $\theta := \partial_t T(\cdot, 0) \in \mathcal{C}^{0,1}_{c,\partial\mathcal{D}_0}(\overline{\mathcal{D}}, \mathbb{R}^2)$. Then, the shape derivative of $\mathcal{J}$ at $\mathbf{\Omega}$ in direction θ is given by*

$$d\mathcal{J}(\mathbf{\Omega})(\theta) = \int_{\mathcal{D}} S_1(\mathbf{\Omega}) : D\theta + S_0(\mathbf{\Omega}) \cdot \theta \, dx, \tag{38}$$

where $S_1(\mathbf{\Omega}) \in L^1(\mathcal{D}, \mathbb{R}^{2\times 2})$ and $S_0(\mathbf{\Omega}) \in L^1(\mathcal{D} \cap supp(\theta), \mathbb{R}^2)$, where $supp(\theta)$ denotes the support of θ, are defined by

$$\begin{aligned} S_1(\mathbf{\Omega}) = &\left[\frac{1}{2}(U-V)^2 + \sigma_{\mathbf{\Omega}}\nabla U \cdot \nabla p + \sigma_{\mathbf{\Omega}}\nabla V \cdot \nabla q\right] I_2 \\ &- \sigma_{\mathbf{\Omega}}\nabla p \otimes \nabla U - \sigma_{\mathbf{\Omega}}\nabla(U-\mathcal{H}) \otimes \nabla p - \sigma_{\mathbf{\Omega}}\nabla q \otimes \nabla V - \sigma_{\mathbf{\Omega}}\nabla(V-\mathcal{H}) \otimes \nabla q, \end{aligned} \tag{39}$$

$$S_0(\mathbf{\Omega}) = \sigma_{\mathbf{\Omega}} D^2\mathcal{H}(\nabla p + \nabla q). \tag{40}$$

The adjoints $p \in H^1_{a,0}(\mathcal{D})$ and $q \in H^1_{b,0}(\mathcal{D})$ are solutions of

$$\int_{\mathcal{D}} \sigma_{\mathbf{\Omega}} \nabla p \cdot \nabla W = -\int_{\mathcal{D}} (U-V)W \quad \textit{for all } W \in H^1_{a,0}(\mathcal{D}), \tag{41}$$

$$\int_{\mathcal{D}} \sigma_{\mathbf{\Omega}} \nabla q \cdot \nabla W = \int_{\mathcal{D}} (U-V)W \quad \textit{for all } W \in H^1_{b,0}(\mathcal{D}). \tag{42}$$

Proof. To prove the shape differentiability, we apply [37, Theorem 2.8], which is based on the implicit function theorem; [37, Theorem 2.8] is provided as Theorem 8 in the Appendix for convenience. Introduce $E = F := H^1_{a,0}(\mathcal{D}) \times H^1_{b,0}(\mathcal{D})$, the dual spaces $E^* = F^* = (H^1_{a,0}(\mathcal{D}))^* \times (H^1_{b,0}(\mathcal{D}))^*$ and the Lagrangian $L : \mathbb{P}_{\mathcal{K}}(\mathcal{D}_0) \times E \times F$ as

$$\begin{aligned} L(\mathbf{\Omega}, (\xi,\zeta), (\mu,\eta)) := &\frac{1}{2}\int_{\mathcal{D}} (\xi-\zeta)^2 + \int_{\mathcal{D}} \sigma_{\mathbf{\Omega}}\nabla\xi \cdot \nabla\mu - \int_{\Gamma_b} g\mu + \int_{\mathcal{D}} \sigma_{\mathbf{\Omega}}\nabla\mathcal{H} \cdot \nabla\mu \\ &+ \int_{\mathcal{D}} \sigma_{\mathbf{\Omega}}\nabla\zeta \cdot \nabla\eta - \int_{\Gamma_a} g\eta + \int_{\mathcal{D}} \sigma_{\mathbf{\Omega}}\nabla\mathcal{H} \cdot \nabla\eta. \end{aligned}$$

In what follows we will write T_t instead of $T(\cdot, t)$ for simplicity. Following the standard procedure in shape optimization, see for instance [37], we introduce the shape-Lagrangian $\mathfrak{L}$ using a reparameterization of L:

$$\mathfrak{L}(t, (\xi,\zeta), (\mu,\eta)) := L(\mathbf{\Omega}_t, (\xi,\zeta) \circ T_t^{-1}, (\mu,\eta) \circ T_t^{-1}) = \langle \mathcal{A}(t,\varphi), \psi \rangle_{F^*,F} + \mathcal{B}(t,\varphi),$$

where the functions $\mathcal{A}$ and $\mathcal{B}$ of (72), see the Appendix, are defined as

$$\begin{aligned}\langle \mathcal{A}(t,(\xi,\zeta)),(\mu,\eta)\rangle_{F^*,F} &:= \int_{\mathcal{D}} \sigma_{\mathbf{\Omega}_t} DT_t^{-\mathsf{T}} \circ T_t^{-1}(\nabla\xi)\circ T_t^{-1} \cdot DT_t^{-\mathsf{T}} \circ T_t^{-1}(\nabla\mu)\circ T_t^{-1} \\ &\quad - \int_{\Gamma_b} g\mu^t + \int_{\mathcal{D}} \sigma_{\mathbf{\Omega}_t} \nabla\mathcal{H}\cdot DT_t^{-\mathsf{T}} \circ T_t^{-1}(\nabla\mu)\circ T_t^{-1} \\ &\quad + \int_{\mathcal{D}} \sigma_{\mathbf{\Omega}_t} DT_t^{-\mathsf{T}} \circ T_t^{-1}(\nabla\zeta)\circ T_t^{-1} \cdot DT_t^{-\mathsf{T}} \circ T_t^{-1}(\nabla\eta)\circ T_t^{-1} \\ &\quad - \int_{\Gamma_a} g\eta^t + \int_{\mathcal{D}} \sigma_{\mathbf{\Omega}_t} \nabla\mathcal{H}\cdot DT_t^{-\mathsf{T}} \circ T_t^{-1}(\nabla\eta)\circ T_t^{-1}, \\ \mathcal{B}(t,(\xi,\zeta)) &:= \frac{1}{2}\int_{\mathcal{D}} (\xi^t-\zeta^t)^2,\end{aligned}$$

with the notation $\xi^t := \xi\circ T_t^{-1}$ and a similar notation for the other functions involved.

Since we have assumed that $\theta = \partial_t T(\cdot,0) \in \mathcal{C}^{0,1}_{c,\partial\mathcal{D}_0}(\overline{\mathcal{D}},\mathbb{R}^2)$, $T_t|_{\partial\mathcal{D}}$ is the identity mapping for all $t\in[0,t_0]$. Proceeding with the change of variables $x\mapsto T_t(x)$ inside the integrals, we get

$$\begin{aligned}\langle \mathcal{A}(t,(\xi,\zeta)),(\mu,\eta)\rangle_{F^*,F} &= \int_{\mathcal{D}} \sigma_{\mathbf{\Omega}}\mathbb{M}(t)\nabla\xi\cdot\nabla\mu - \int_{\Gamma_b} g\mu + \int_{\mathcal{D}} \sigma_{\mathbf{\Omega}}\nabla\mathcal{H}\circ T_t \cdot DT_t^{-\mathsf{T}}\nabla\mu\det(DT_t) \\ &\quad + \int_{\mathcal{D}} \sigma_{\mathbf{\Omega}}\mathbb{M}(t)\nabla\zeta\cdot\nabla\eta - \int_{\Gamma_a} g\eta + \int_{\mathcal{D}} \sigma_{\mathbf{\Omega}}\nabla\mathcal{H}\circ T_t \cdot DT_t^{-\mathsf{T}}\nabla\eta\det(DT_t), \\ \mathcal{B}(t,(\xi,\zeta)) &= \frac{1}{2}\int_{\mathcal{D}} (\xi-\zeta)^2\det(DT_t),\end{aligned}$$

where $\mathbb{M}(t) := \det(DT_t)DT_t^{-1}DT_t^{-\mathsf{T}}$. Using $\theta\in\mathcal{C}^{0,1}_{c,\partial\mathcal{D}_0}(\overline{\mathcal{D}},\mathbb{R}^2)$ and Assumption 1, we have $t\mapsto T_t\in\mathcal{C}^1([0,t_0],\mathcal{C}^{0,1}(\overline{\mathcal{D}},\mathbb{R}^2))$ and the following standard results, see for instance [37, Lemma 2.7],

$$\begin{aligned}&t\mapsto DT_t\in\mathcal{C}^1([0,t_0],L^\infty(\mathcal{D},\mathbb{R}^{2\times2})) \text{ with } DT_0=I_2 \text{ and } \partial_t DT_t|_{t=0}=D\theta,\\ &t\mapsto DT_t^{-1}\in\mathcal{C}^1([0,t_0],L^\infty(\mathcal{D},\mathbb{R}^{2\times2})) \text{ with } \partial_t DT_t^{-1}|_{t=0}=-D\theta,\\ &t\mapsto \det(DT_t)\in\mathcal{C}^1([0,t_0],L^\infty(\mathcal{D})), \det(DT_t)|_{t=0}=1 \text{ and } \partial_t\det(DT_t)|_{t=0}=\operatorname{div}(\theta).\end{aligned}$$

Thus $t\mapsto\mathbb{M}(t)\in\mathcal{C}^1([0,t_0],L^\infty(\mathcal{D},\mathbb{R}^{2\times2}))$ and we obtain

$$\mathbb{M}'(0) = \operatorname{div}(\theta)I_2 - D\theta - D\theta^{\mathsf{T}}. \tag{43}$$

By standard elliptic regularity, $\mathcal{H}\in H^2(\mathcal{O})$, where $\mathcal{O}$ is any open set such that $\overline{\mathcal{O}}\subset\mathcal{D}$. Since $\theta\in\mathcal{C}^{0,1}_{c,\partial\mathcal{D}_0}(\overline{\mathcal{D}},\mathbb{R}^2)$, i.e., θ has compact support in $\mathcal{D}$, we get that $\nabla\mathcal{H}\circ T_t$ is differentiable with respect to t, and

$$\frac{d}{dt}\nabla\mathcal{H}\circ T_t\Big|_{t=0} = (D^2\mathcal{H})\theta.$$

Gathering these results, we conclude that $\mathcal{A}\in\mathcal{C}^1([0,t_0]\times E,F^*)$ and $\mathcal{B}\in\mathcal{C}^1([0,t_0]\times E,\mathbb{R})$. This allows us to apply Theorem 8, see the Appendix. We identify $A := \partial_{(\xi,\zeta)}\mathcal{A}(0,(\bar U,\bar V))\in\mathcal{L}(E,F^*)$ as

$$\langle A(\hat\xi,\hat\zeta),(\mu,\eta)\rangle_{F^*,F} = \int_{\mathcal{D}}\sigma_{\mathbf{\Omega}}\nabla\hat\xi\cdot\nabla\mu + \int_{\mathcal{D}}\sigma_{\mathbf{\Omega}}\nabla\hat\zeta\cdot\nabla\eta,$$

then $L((\bar U,\bar V)) := \partial_t\mathcal{A}(0,(\bar U,\bar V))\in F^*$ as

$$\begin{aligned}\langle L((\bar U,\bar V)),(\mu,\eta)\rangle_{F^*,F} &= \int_{\mathcal{D}}\sigma_{\mathbf{\Omega}}\mathbb{M}'(0)\nabla\bar U\cdot\nabla p + \int_{\mathcal{D}}\sigma_{\mathbf{\Omega}}\mathbb{M}'(0)\nabla\bar V\cdot\nabla q \\ &\quad + \int_{\mathcal{D}}\sigma_{\mathbf{\Omega}}(D^2\mathcal{H})\theta\cdot\nabla p - \sigma_{\mathbf{\Omega}}\nabla\mathcal{H}\cdot D\theta^{\mathsf{T}}\nabla p + \sigma_{\mathbf{\Omega}}\nabla\mathcal{H}\cdot\nabla p\operatorname{div}(\theta) \\ &\quad + \int_{\mathcal{D}}\sigma_{\mathbf{\Omega}}(D^2\mathcal{H})\theta\cdot\nabla q - \sigma_{\mathbf{\Omega}}\nabla\mathcal{H}\cdot D\theta^{\mathsf{T}}\nabla q + \sigma_{\mathbf{\Omega}}\nabla\mathcal{H}\cdot\nabla q\operatorname{div}(\theta)\end{aligned}$$

and

$$\langle B((\bar U,\bar V)),(\hat\xi,\hat\zeta)\rangle_{E^*,E} := \langle \partial_{(\xi,\zeta)}\mathcal{B}(0,(\bar U,\bar V)),(\hat\xi,\hat\zeta)\rangle_{E^*,E} = \int_{\mathcal{D}} (\bar U-\bar V)(\hat\xi-\hat\zeta).$$

Gathering these results and using (75) yields

$$\begin{aligned} d\mathcal{J}(\mathbf{\Omega})(\theta) &= \partial_t \mathfrak{L}(0,(\bar U,\bar V),(p,q)) = \langle L((\bar U,\bar V)),(p,q)\rangle_{F^*,F} + \partial_t\mathcal{B}(0,(\bar U,\bar V)) \\ &= \frac{1}{2}\int_{\mathcal{D}} (\bar U-\bar V)^2 \operatorname{div}(\theta) + \int_{\mathcal{D}} \sigma_{\mathbf{\Omega}} \mathbb{M}'(0)\nabla\bar U\cdot\nabla p + \int_{\mathcal{D}} \sigma_{\mathbf{\Omega}}\mathbb{M}'(0)\nabla\bar V\cdot\nabla q \\ &\quad + \int_{\mathcal{D}} \sigma_{\mathbf{\Omega}}(D^2\mathcal{H})\theta\cdot\nabla p - \sigma_{\mathbf{\Omega}}\nabla\mathcal{H}\cdot D\theta^{\mathsf{T}}\nabla p + \sigma_{\mathbf{\Omega}}\nabla\mathcal{H}\cdot\nabla p\operatorname{div}(\theta) \\ &\quad + \int_{\mathcal{D}} \sigma_{\mathbf{\Omega}}(D^2\mathcal{H})\theta\cdot\nabla q - \sigma_{\mathbf{\Omega}}\nabla\mathcal{H}\cdot D\theta^{\mathsf{T}}\nabla q + \sigma_{\mathbf{\Omega}}\nabla\mathcal{H}\cdot\nabla q\operatorname{div}(\theta). \end{aligned}$$

Using (43) and standard tensor calculus, see for instance [37, Section 2.1], we compute

$$\mathbb{M}'(0)\nabla\bar U\cdot\nabla p = D\theta : [(\nabla\bar U\cdot\nabla p)I_2 - \nabla p\otimes\nabla\bar U - \nabla\bar U\otimes\nabla p].$$

The other terms of $d\mathcal{J}(\mathbf{\Omega})(\theta)$ can be rearranged in a similar way. Using also the relations $U=\bar U+\mathcal{H}$ and $V=\bar V+\mathcal{H}$, we obtain (38).

Finally, the regularity $S_1(\mathbf{\Omega})\in L^1(\mathcal{D},\mathbb{R}^{2\times 2})$ follows immediately in view of the regularity of U,V,p,q. To obtain $S_0(\mathbf{\Omega})\in L^1(\mathcal{D}\cap\operatorname{supp}(\theta),\mathbb{R}^2)$ we use the regularity of U,V,p,q, but we also need $\mathcal{H}\in H^2(\mathcal{O})$, where $\mathcal{O}$ is any open set such that $\overline{\mathcal{O}}\subset\mathcal{D}$ and the fact that $\theta\in\mathcal{C}^{0,1}_{c,\partial\mathcal{D}_0}(\overline{\mathcal{D}},\mathbb{R}^2)$ has compact support in $\mathcal{D}$. □

4.1 Interface representation of the gradient

We now investigate the case where $\mathbf{\Omega}$ is a Voronoi diagram, considering the framework of Section 3.2. We assume $\mathbf{\Omega}(\mathbf{a})\in\mathbb{P}_{\mathcal{K}_{\mathrm{vor}}}(\mathcal{D}_0)$ is a Voronoi diagram associated with $\mathbf{a}$. The key ingredient to obtain an interface representation of the gradient in Theorem 2 is the higher regularity $S_1(\mathbf{\Omega}(\mathbf{a}))|_{\Omega_i(\mathbf{a})}\in W^{1,1}(\Omega_i(\mathbf{a}),\mathbb{R}^{2\times 2})$ for all $i\in\mathcal{K}_{\mathrm{vor}}=\{1,\dots,\kappa_0\}$. The main reason is that it allows us to apply the divergence theorem and thus transform the distributed expression (38) into a sum of integrals over the edges of the diagram. However, proving such higher regularity is not immediate due to the nonsmoothness of the cells $\Omega_i(\mathbf{a})$. In a smooth set, the regularity of U,V only depends on the regularity of the data f,g,h, but for a transmission problem with polygonal cells, it is known [42, 43] that weak singularities appear at the corners of each cell $\Omega_i(\mathbf{a})$, which imposes a limit on the regularity of U,V,p,q. In [14, Section 4.1] we also obtained an interface representation of the gradient by establishing higher regularity for the state and adjoint. Compared to [14, Section 4.1], proving higher regularity for conductivity problems is more challenging as the singularities appearing at the corners are stronger.

We first provide some explanations about these weak singularities. The following result is a straightforward adaptation to our setting of [41, Lemma 1], see [43] for a proof. Let $\mathcal{V}$ be the set of vertices of the Voronoi diagram $\mathbf{\Omega}(\mathbf{a})$; note that $\partial\mathcal{D}\cap\mathcal{V}=\emptyset$ since the cells of $\mathbf{\Omega}(\mathbf{a})$ are included in $\mathcal{D}_0$. Let $\eta_v:\mathcal{D}\to\mathbb{R}$ be a cut-off function equal to 1 near $v\in\mathcal{V}$ whose support does not contain the other vertices. Recall that $\mathcal{D}_{\hat\delta}$ is defined in (27), for $0<\hat\delta<\delta$. We consider the following model problem: let $u\in H^1_{a,h}(\mathcal{D})$ be the solution of

$$\int_{\mathcal{D}} \sigma_{\mathbf{\Omega}(\mathbf{a})}\nabla u\cdot\nabla W = \int_{\mathcal{D}} fW + \int_{\Gamma_b} gW \quad \text{for all } W\in H^1_{a,0}(\mathcal{D}), \tag{44}$$

with $\overline{\Gamma_a}\cup\overline{\Gamma_b}=\partial\mathcal{D}$, $\Gamma_a\neq\emptyset$, $f\in L^2(\mathcal{D})$, $g\in L^2(\partial\mathcal{D})$, $h\in H^{1/2}(\partial\mathcal{D})$ and

$$H^1_{a,h}(\mathcal{D}) := \{W\in H^1(\mathcal{D}) \mid W=h \text{ on } \Gamma_a\}.$$

Choosing the appropriate data, the functions U,V,p,q can be modeled by (44). Note that in [41], homogeneous Dirichlet conditions for u are considered on $\partial\mathcal{D}$, but this is not relevant here as we are only interested in singularities occurring at a positive distance from the boundary $\partial\mathcal{D}$, for which the results of [41] also hold. In the case of conductivity problem with internal measurements, we will consider homogeneous Dirichlet conditions for u, see Section 5.

Lemma 1 ([41]). *Let $f \in L^2(\mathcal{D})$, for any $\hat{\delta}$ such that $0 < \hat{\delta} < \delta$, the restriction to $\mathcal{D}_{\hat{\delta}}$ of the solution u to (44) admits the following decomposition*

$$u|_{\mathcal{D}_{\hat{\delta}}} = u_r + u_s \text{ with } u_s := \sum_{v \in \mathcal{V}} \eta_v \sum_{\alpha \in \Lambda_v} c_\alpha^v S_\alpha^v, \tag{45}$$

where $u_r|_{\Omega_i(\mathbf{a})} \in H^2(\Omega_i(\mathbf{a}))$, $i \in \mathcal{K}_{vor}$, $u_r|_{\Omega_0 \cap \mathcal{D}_{\hat{\delta}}} \in H^2(\Omega_0 \cap \mathcal{D}_{\hat{\delta}})$, Λ_v is a finite set of positive real numbers, c_α^v are constants and S_α^v are vertex singular functions independent of f. These functions, expressed in polar coordinates (r_v, ϑ_v) centered at v, are of the form

$$S_\alpha^v = r_v^\alpha \Phi_\alpha^v(\vartheta_v). \tag{46}$$

Let C_i^v, $i \in \mathcal{K}_{vor} \cup \{0\}$, be the cone coinciding with $\Omega_i(\mathbf{a})$ or Ω_0 in a neighborhood of v. The restrictions $S_\alpha^v|_{C_i^v}$ are smooth with respect to the second variable ϑ_v.

The purpose of $\mathcal{D}_{\hat{\delta}}$ in Lemma 1 is to avoid the singularities occurring at the vertices of $\partial\mathcal{D}$. Note that a description of such singularities can also be obtained if needed, using for instance the results of [41]. Then we have the following result, see [41, Corollary 2].

Corollary 2. *Suppose that the assumptions of Lemma 1 hold, then for all $s < \alpha_v := \min_{\alpha \in \Lambda_v} \alpha$, one has*

$$\eta_v u|_{\Omega_i(\mathbf{a})} \in H^{1+s}(\Omega_i(\mathbf{a})), \qquad \forall i \in \mathcal{K}_{vor}$$

and $\eta_v u|_{\Omega_0 \cap \mathcal{D}_{\hat{\delta}}} \in H^{1+s}(\Omega_0 \cap \mathcal{D}_{\hat{\delta}})$, for any $\hat{\delta}$ such that $0 < \hat{\delta} < \delta$.

In view of (26) and Assumption 2, for δ sufficiently small, the cells $\Omega_i(\mathbf{a})$ are at a positive distance to $\partial\mathcal{D}$, for all $i \in \mathcal{K}_{\rm vor}$, hence Ω_0 plays the role of an insulating layer, separating $\partial\mathcal{D}$ from the cells of the Voronoi diagram; see Figure 1. As mentioned above, the motivation for this assumption in EIT is to avoid regularity issues that would occur with the solutions U, V, p, q in the case where the boundary of some cell $\Omega_i(\mathbf{a})$, $i \in \mathcal{K}_{\rm vor}$, would touch the boundary of $\mathcal{D}$. In view of this observation, Lemma 1 and Corollary 2, we obtain the following result.

Proposition 1. *Suppose Assumptions 2 and 3 hold and $\sigma_i, i \in \mathcal{K}_{vor}$, are constant. Then $S_1(\mathbf{\Omega}(\mathbf{a}))|_{\Omega_i(\mathbf{a})} \in W^{1,1}(\Omega_i(\mathbf{a}), \mathbb{R}^{2\times 2})$ for all $i \in \mathcal{K}_{vor}$, $S_1(\mathbf{\Omega}(\mathbf{a}))|_{\Omega_0 \cap \mathcal{D}_\delta} \in W^{1,1}(\Omega_0 \cap \mathcal{D}_{\hat{\delta}}, \mathbb{R}^{2\times 2})$ for all $0 < \hat{\delta} < \delta$, where $S_1(\mathbf{\Omega}(\mathbf{a}))$ is given in (39).*

Proof. For simplicity, we will omit the restriction to $\Omega_i(\mathbf{a})$ in the notation, for instance we write $S_1(\mathbf{\Omega}(\mathbf{a}))$ instead of $S_1(\mathbf{\Omega}(\mathbf{a}))|_{\Omega_i(\mathbf{a})}$. Using Assumption 2, the interior vertex $v \in \mathcal{V}$ belongs to the boundary of at most three phases. We start with the case where $v \in \mathcal{V}$ belongs to exactly two phases. In view of [41, Theorem 16(ii)], we have $\alpha_v > 1/2$ in this case, where α_v is defined in Corollary 2. To prove $S_1(\mathbf{\Omega}(\mathbf{a})) \in W^{1,1}(\Omega_i(\mathbf{a}), \mathbb{R}^{2\times 2})$, for some given $i \in \mathcal{K}_{\rm vor}$, it is sufficient to prove that

$$DS_1(\mathbf{\Omega}(\mathbf{a})) \in L^1(\Omega_i(\mathbf{a}), \mathbb{R}^{2\times 2\times 2}),$$

as $S_1(\mathbf{\Omega}(\mathbf{a})) \in L^1(\Omega_i(\mathbf{a}), \mathbb{R}^{2\times 2})$ is proved in a similar way. In view of (39), the most singular terms in $DS_1(\mathbf{\Omega}(\mathbf{a}))$ are $D^2U\nabla p$, $D^2V\nabla q$, $D^2p\nabla U$, $D^2q\nabla V$, $D^2\mathcal{H}\nabla p$, $D^2\mathcal{H}\nabla q$, $D^2p\nabla\mathcal{H}$, $D^2q\nabla\mathcal{H}$. Thus, it is sufficient to prove that $D^2U\nabla p, D^2\mathcal{H}\nabla p, D^2p\nabla\mathcal{H} \in L^1(\Omega_i(\mathbf{a}), \mathbb{R}^2)$ for instance, as the other terms can be treated in a similar way. We start with $D^2U\nabla p$. Applying Lemma 1 to U, p and in view of (45), we have

$$D^2U\nabla p = D^2U_r\nabla p + D^2U_s\nabla p_r + D^2U_s\nabla p_s.$$

Since $U_r \in H^2(\Omega_i(\mathbf{a}))$ and $p \in H^1(\Omega_i(\mathbf{a}))$ we get $D^2U_r\nabla p \in L^1(\Omega_i(\mathbf{a}), \mathbb{R}^2)$. Since U_s is a sum of functions of the type (46), with $\alpha \geq \alpha_v$, to show $D^2U_s\nabla p_r \in L^1(\Omega_i(\mathbf{a}), \mathbb{R}^2)$ it is sufficient to prove $D^2(r_v^{\alpha_v})\nabla p_r \in L^1(\Omega_i(\mathbf{a}), \mathbb{R}^2)$, which is also equivalent to proving $r_v^{\alpha_v - 2}\nabla p_r \in L^1(\Omega_i(\mathbf{a}), \mathbb{R}^2)$. Using the Cauchy-Schwarz inequality we have

$$\left(\int_{\Omega_i(\mathbf{a})} r_v^{\alpha_v - 2}\nabla p_r\right)^2 \leq \int_{\Omega_i(\mathbf{a})} |r_v^{\alpha_v - 1}|^2 \int_{\Omega_i(\mathbf{a})} |r_v^{-1}\nabla p_r|^2 < \infty.$$

Indeed, $\int_{\Omega_i(\mathbf{a})} |r_v^{\alpha_v - 1}|^2 < \infty$ due to $\alpha_v > 1/2$. For the other integral, we have $r_v^{-1} \nabla p_r \in L^2(\Omega_i(\mathbf{a}), \mathbb{R}^2)$ due to $\nabla p_r \in H^1(\Omega_i(\mathbf{a}), \mathbb{R}^2)$ and Hardy's inequality, see [23, Theorem 1.4.4.4]. This shows that $r_v^{\alpha_v - 2} \nabla p_r \in L^1(\Omega_i(\mathbf{a}), \mathbb{R}^2)$, hence also $D^2 U_s \nabla p_r \in L^1(\Omega_i(\mathbf{a}), \mathbb{R}^2)$.

To prove $D^2 U_s \nabla p_s \in L^1(\Omega_i(\mathbf{a}), \mathbb{R}^2)$, using again the fact that U_s and p_s are both sums of functions of the type (46), with $\alpha \geq \alpha_v$, it is sufficient to prove that $D^2(r_v^{\alpha_v}) \nabla (r_v^{\alpha_v}) \in L^1(\Omega_i(\mathbf{a}), \mathbb{R}^2)$, or equivalently that $r_v^{\alpha_v - 2} r_v^{\alpha_v - 1} = r_v^{2\alpha_v - 3} \in L^1(\Omega_i(\mathbf{a}), \mathbb{R}^2)$. Since $\alpha_v > 1/2$ we have indeed $r_v^{2\alpha_v - 3} \in L^1(\Omega_i(\mathbf{a}), \mathbb{R}^2)$.

Gathering these results we have shown that $D^2 u \nabla p \in L^1(\Omega_i(\mathbf{a}), \mathbb{R}^{2\times 2})$, then proceeding similarly for the other term we obtain $S_1(\mathbf{\Omega}(\mathbf{a})) \in W^{1,1}(\Omega_i(\mathbf{a}), \mathbb{R}^{2\times 2})$. For the terms depending on $\mathcal{H}$ such as $D^2 \mathcal{H} \nabla p$, we use the fact that $\mathcal{H} \in H^2(\mathcal{O})$, where $\mathcal{O}$ is any open set such that $\overline{\mathcal{O}} \subset \mathcal{D}$.

We now treat the case where $v \in \mathcal{V}$ belongs to exactly three phases $\Omega_i(\mathbf{a}), \Omega_j(\mathbf{a}), \Omega_k(\mathbf{a})$. If the coefficients $\sigma_i, \sigma_j, \sigma_k$ are not pairwise distinct then we can merge the cells with the same coefficients and conclude using the results for the case treated above, where $v \in \mathcal{V}$ belongs to exactly two phases.

Next we assume that the coefficients $\sigma_i, \sigma_j, \sigma_k$ are pairwise distinct. In view of [41, Theorem 16(iii)], we have

$$\alpha_v > \min\left(\frac{1}{2}, \frac{\pi}{2\gamma^v}\right),$$

where γ^v is the interior angle of one of the three phases $\Omega_i(\mathbf{a}), \Omega_j(\mathbf{a}), \Omega_k(\mathbf{a})$ at the vertex $v \in \mathcal{V}$, corresponding to the coefficient σ_i, σ_j or σ_k that is not an extrema in $\{\sigma_i, \sigma_j, \sigma_k\}$. Since the cells of the Voronoi diagram are convex, we have $\gamma^v < \pi$, hence $\alpha_v > 1/2$. Thus, proceeding as in the case where v belongs to the boundary of exactly two phases, we obtain $S_1(\mathbf{\Omega}(\mathbf{a})) \in W^{1,1}(\Omega_i(\mathbf{a}), \mathbb{R}^{2\times 2})$.

Finally, the fact that $S_1(\mathbf{\Omega}(\mathbf{a}))|_{\Omega_0 \cap \mathcal{D}_{\hat{\delta}}} \in W^{1,1}(\Omega_0 \cap \mathcal{D}_{\hat{\delta}}, \mathbb{R}^2)$ for all $0 < \hat{\delta} < \delta$ is also obtained via Lemma 1. One uses the decomposition (45) and proceeds in a similar way as for the other phases. Note that in this case the relevant interior vertices belong either to the boundary of two phases or to the boundary of three phases. In the latter case we have $\gamma^v \leq \pi$, see Figure 1, hence $\alpha_v > 1/2$ and the result is the same as for the other phases. □

Using the regularity provided by Proposition 1 we can apply Theorem 2, and in combination with Theorem 3 we obtain the following result.

Theorem 4. *Suppose Assumptions 2 and 3 hold, then the gradient of $G(\mathbf{a})$, defined in (16), is given by*

$$\nabla G(\mathbf{a}) \cdot \delta \mathbf{a} = \sum_{i \in \mathcal{K}_{vor}} \sum_{E \in \mathcal{E}_i^{\text{int}}} \int_E (S_1(\mathbf{\Omega}(\mathbf{a}))\nu \cdot \nu)|_{\Omega_i(\mathbf{a})} \frac{(x - a_i) \cdot \delta a_i - (x - a_{k(i,E)}) \cdot \delta a_{k(i,E)}}{\|a_{k(i,E)} - a_i\|} dx, \tag{47}$$

where $k(i,E)$ is the index such that $E = \overline{\Omega_i(\mathbf{a})} \cap \overline{\Omega_{k(i,E)}(\mathbf{a})}$, $\mathcal{E}_i^{\text{int}}$ the set of interior edges of the cell $\Omega_i(\mathbf{a})$ with respect to $\mathcal{D}_0$ and $S_1(\mathbf{\Omega}(\mathbf{a}))$ is given by (39).

The gradient $\nabla G(\mathbf{a})$ may be simplified using the regularity of some of the terms in $S_1(\mathbf{\Omega}(\mathbf{a}))\nu \cdot \nu$ across the edges of the diagram. This leads to the following expression of the gradient.

Corollary 3. *Suppose Assumptions 2 and 3 hold, then*

$$\nabla G(\mathbf{a}) \cdot \delta \mathbf{a} = \sum_{i \in \mathcal{K}_{vor}} \sum_{E \in \mathcal{E}_i^{\text{int}}} \delta a_{k(i,E)} \cdot \lambda_{k,E} + \delta a_i \cdot \lambda_{i,E}, \tag{48}$$

with

$$\lambda_{k,E} = -\int_E \mathfrak{S}_i \frac{(x - a_{k(i,E)})}{\|a_{k(i,E)} - a_i\|} dx, \qquad \lambda_{i,E} = \int_E \mathfrak{S}_i \frac{(x - a_i)}{\|a_{k(i,E)} - a_i\|} dx$$

and

$$\mathfrak{S}_i := \sigma_i(\nabla U \cdot \nabla p + \nabla V \cdot \nabla q) + \sigma_i(-\partial_\nu p \partial_\nu U - \partial_\nu q \partial_\nu V - \partial_\nu p \partial_\nu (U - \mathcal{H}) - \partial_\nu q \partial_\nu (V - \mathcal{H})). \tag{49}$$

Proof. Let $\mathcal{E} := \cup_{i \in \mathcal{K}_{\text{vor}}} \mathcal{E}_i^{\text{int}}$ denote the set of interior edges of the Voronoi diagram (i.e., edges that are included in $\mathcal{D}_0$). Firstly, we can write $\nabla G(\mathbf{a})$ as in (35). Then, as each interior edge $E \in \mathcal{E}$ is at the

interface of exactly two cells, whose indices we denote by $k_1(E)$ and $k_2(E)$, we can reorganize the terms in (35) by summing over all $E \in \mathcal{E}$, which yields:

$$\nabla G(\mathbf{a}) \cdot \delta\mathbf{a} = \sum_{E \in \mathcal{E}} \delta a_{k_1(E)} \cdot \lambda_{k_1,E} + \delta a_{k_2(E)} \cdot \lambda_{k_2,E}, \tag{50}$$

where

$$\lambda_{k_1,E} := \int_E [\![S_1(\mathbf{\Omega}(\mathbf{a}))\nu \cdot \nu]\!]_E \frac{(x - a_{k_1(E)})}{\|a_{k_1(E)} - a_{k_2(E)}\|} dx,$$
$$\lambda_{k_2,E} := -\int_E [\![S_1(\mathbf{\Omega}(\mathbf{a}))\nu \cdot \nu]\!]_E \frac{(x - a_{k_2(E)})}{\|a_{k_1(E)} - a_{k_2(E)}\|} dx,$$

and with the jumps

$$[\![S_1(\mathbf{\Omega}(\mathbf{a}))\nu \cdot \nu]\!]_E := (S_1(\mathbf{\Omega}(\mathbf{a}))\nu \cdot \nu)|_{\partial\Omega_{k_1(E)}(\mathbf{a})} - (S_1(\mathbf{\Omega}(\mathbf{a}))\nu \cdot \nu)|_{\partial\Omega_{k_2(E)}(\mathbf{a})}.$$

In view of (39) we have

$$\begin{aligned} S_1(\mathbf{\Omega}(\mathbf{a}))\nu \cdot \nu = &\frac{1}{2}(U - V)^2 + \sigma_{\mathbf{\Omega}}(\nabla U \cdot \nabla p + \nabla V \cdot \nabla q) \\ &+ \sigma_{\mathbf{\Omega}}(-\partial_\nu p \partial_\nu U - \partial_\nu q \partial_\nu V - \partial_\nu p \partial_\nu (U - \mathcal{H}) - \partial_\nu q \partial_\nu (V - \mathcal{H})). \end{aligned} \tag{51}$$

Since $U, V \in H^1(\mathcal{D})$, we can prove that

$$[\![\frac{1}{2}(U - V)^2]\!]_E = 0.$$

Indeed, we have $(U - V)^2 \in W^{1,1}(\mathcal{D})$, hence $(U - V)^2|_{\Omega_i(\mathbf{a})} \in W^{1,1}(\Omega_i(\mathbf{a}))$ for all $i \in \mathcal{K}_{\text{vor}}$. Since $\Omega_i(\mathbf{a})$ is Lipschitz, the trace $\text{Tr} : W^{1,1}(\Omega_i(\mathbf{a})) \to L^1(\partial\Omega_i(\mathbf{a}))$ is linear and continuous, see [34], thus $(U - V)^2|_{\partial\Omega_i(\mathbf{a})} \in L^1(\partial\Omega_i(\mathbf{a}))$. In addition, since $(U - V)^2 \in W^{1,1}(\mathcal{D})$ and using the continuity of the trace Tr, we have $(U - V)^2|_{\partial\Omega_i(\mathbf{a})} = (U - V)^2|_{\partial\Omega_j(\mathbf{a})}$ on the interface $E = \partial\Omega_i(\mathbf{a}) \cap \partial\Omega_j(\mathbf{a})$, for all $i, j \in \mathcal{K}_{\text{vor}}$. Therefore, $[\![(U - V)^2]\!]_E = 0$.

Thus, we have show at

$$\begin{aligned} [\![S_1(\mathbf{\Omega}(\mathbf{a}))\nu \cdot \nu]\!]_E = &[\![\sigma_{\mathbf{\Omega}}(\nabla U \cdot \nabla p + \nabla V \cdot \nabla q)]\!]_E \\ &+ [\![\sigma_{\mathbf{\Omega}}(-\partial_\nu p \partial_\nu U - \partial_\nu q \partial_\nu V - \partial_\nu p \partial_\nu (U - \mathcal{H}) - \partial_\nu q \partial_\nu (V - \mathcal{H}))]\!]_E. \end{aligned}$$

Finally, rewriting the sum as in (35), we obtain (48), (49). □

4.2 Example of a singular case

Here we discuss the case where Assumption 2 does not hold, which creates two difficulties. The first issue is that, following the theory developed in [13], the motion of the Voronoi cell $\Omega_i(\mathbf{a} + t\delta\mathbf{a})$ can be parameterized by a bi-Lipschitz mapping $T(\cdot, t)$ under Assumption 2, which is crucial to prove shape differentiability, see Theorem 1. If Assumption 2 does not hold, the existence of such mapping is not guaranteed. Nevertheless, when Assumption 2 does not hold one can still perform the sensitivity analysis of $\mathbf{a} \mapsto \mathbf{\Omega}(\mathbf{a})$ in specific cases using asymptotic analysis, as in [13, Example 8] in the case of cost functionals that do not depend on the solution to a PDE. The second issue is related to the shape functional $\mathbf{\Omega} \mapsto \mathcal{J}(\mathbf{\Omega})$ and is specific to the PDE case. When Assumption 2 does not hold, more than three phases may meet at a vertex of the Voronoi diagram, which results in a stronger singularity in a neighborhood of the vertex, as predicted by the theory of weak singularities in corner domains [41, 42, 43]. We illustrate these issues with a particular singular configuration similar to [13, Example 8].

Example 1. *Let $\mathcal{D} = (-1, 1)^2$, $\mathcal{K}_{vor} = \{1, 2, 3, 4\}$, and consider the Voronoi diagram with $a_1 + t\delta a_1 = (1/2 + t, 0)$, $a_2 = (0, 1/2)$, $\delta a_2 = 0$, $a_3 + t\delta a_3 = (-1/2 - t, 0)$, $a_4 = (0, -1/2)$, $\delta a_4 = 0$, where $t \geq 0$ is a small parameter; see Figure 2. Assumption 2 does not hold for this configuration. For $t > 0$, we compute*

$$\overline{\Omega_1(\mathbf{a} + t\delta\mathbf{a})} \cap \overline{\Omega_2(\mathbf{a} + t\delta\mathbf{a})} \cap \overline{\Omega_4(\mathbf{a} + t\delta\mathbf{a})} = \left\{ \left(\frac{t + t^2}{1 + 2t}, 0 \right) \right\},$$
$$\overline{\Omega_2(\mathbf{a} + t\delta\mathbf{a})} \cap \overline{\Omega_3(\mathbf{a} + t\delta\mathbf{a})} \cap \overline{\Omega_4(\mathbf{a} + t\delta\mathbf{a})} = \left\{ \left(-\frac{t + t^2}{1 + 2t}, 0 \right) \right\}.$$

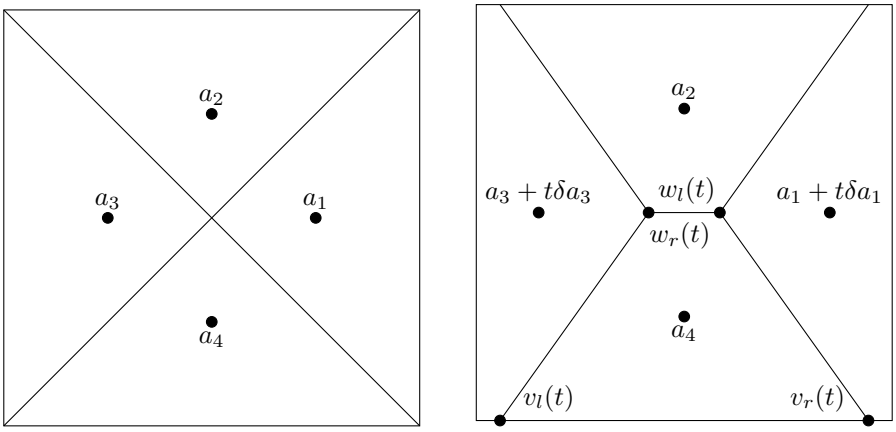

Figure 2: On the left, the four phases $\Omega_i(\mathbf{a})$, $i \in \mathcal{K}_{\rm vor} = \{1,2,3,4\}$ at $t = 0$ with the quadruple point $(0,0)$ in the center. On the right, the four phases at $t > 0$, illustrating how the quadruple point $(0,0)$ at $t = 0$ splits into two stable triple points $\left(\pm\frac{t+t^2}{1+2t}, 0\right)$ at $t > 0$.

This illustrates the instability of the quadruple point $\{(0,0)\}$ *at* $t = 0$*, which immediately splits into two stable triple points* $\left(\pm\frac{t+t^2}{1+2t}, 0\right)$ *for* $t > 0$*.*

The key property to obtain the Hadamard-type formula (31) in Theorem 2, or (47) in Theorem 4, is the higher regularity $S_1(\mathbf{\Omega}(\mathbf{a}))|_{\Omega_i(\mathbf{a})} \in W^{1,1}(\Omega_i(\mathbf{a}), \mathbb{R}^{2\times 2})$ for all $i \in \mathcal{K}_{\rm vor}$, which was proved in Proposition 1 under Assumption 2. When Assumption 2 does not hold as in Example 1, the higher regularity $S_1(\mathbf{\Omega}(\mathbf{a}))|_{\Omega_i(\mathbf{a})} \in W^{1,1}(\Omega_i(\mathbf{a}), \mathbb{R}^{2\times 2})$ may fail, as a consequence of the following result.

Proposition 2. *Suppose Assumption 3 holds,* $\sigma_i, i \in \mathcal{K}_{vor}$*, are constants and the geometry is defined as in Example 1 (for* $t = 0$*), then* $\alpha_v > 1/3$*, where* α_v *is given in Corollary 2.*

Proof. We apply the results of [41, Theorem 16], where three cases are separated when four or more cells have a common vertex. The first case corresponds to a decreasing sequence $\sigma_i, i \in \mathcal{K}_{\rm vor}$, the second case to an increasing sequence $\sigma_i, i \in \mathcal{K}_{\rm vor}$, and in the last case, the sequence $\sigma_i, i \in \mathcal{K}_{\rm vor}$ is not monotonous. Let $\mathcal{K}_{\rm vor} = \{1,2,3,4\}$ and $\omega_i - \omega_{i-1}$ be the angle of the cell $\Omega_i(\mathbf{a})$ at the vertex $S = (0,0)$, with $0 = \omega_0 < \omega_1 < \omega_2 < \omega_3 < \omega_4 = 2\pi$. In Example 1, at $t = 0$, we have $\omega_1 = \pi/2$, $\omega_2 = \pi$, $\omega_3 = 3\pi/2$.

According to [41, Theorem 16(i)(a)], if $\sigma_i, i \in \mathcal{K}_{\rm vor}$, is a decreasing sequence we have

$$\alpha_v > \min\left(\frac{1}{2}, \frac{\pi}{2\omega_3}\right) = \frac{1}{3}$$

and if $\sigma_i, i \in \mathcal{K}_{\rm vor}$, is an increasing sequence we have

$$\alpha_v > \min\left(\frac{1}{2}, \frac{\pi}{2(2\pi - \omega_1)}\right) = \frac{1}{3}.$$

If $\sigma_i, i \in \mathcal{K}_{\rm vor}$, is not monotonous we also get $\alpha_v > 1/3$ using [41, Theorem 16(i)(c)]. □

Proposition 2 implies that $S_1(\mathbf{\Omega}(\mathbf{a}))|_{\Omega_i(\mathbf{a})}$ does not belong to $W^{1,1}(\Omega_i(\mathbf{a}), \mathbb{R}^{2\times 2})$ in general. Indeed, as discussed in the proof of Proposition 1, the most singular terms in $DS_1(\mathbf{\Omega}(\mathbf{a}))$ are $D^2U\nabla p$, $D^2V\nabla q$, $D^2p\nabla U$, $D^2q\nabla V$, $D^2\mathcal{H}\nabla p$, $D^2\mathcal{H}\nabla q$, $D^2p\nabla\mathcal{H}$, $D^2q\nabla\mathcal{H}$. Consider for instance $D^2U\nabla p$: in view of expansion (45), the most singular term in $D^2U\nabla p$ is $D^2(r_v^{\alpha_v})\nabla(r_v^{\alpha_v})$ which behaves like $r_v^{\alpha_v-3}$ and since $\alpha_v - 3 > -7/3$, we have $r_v^{\alpha_v-3} \notin W^{1,1}(\Omega_i(\mathbf{a}), \mathbb{R}^{2\times 2})$. Thus, in general we cannot apply Theorem 2 in the geometric configuration of Example 1 to obtain the Hadamard-type formula (31). To prove or disprove shape differentiability, one would have to conduct an asymptotic analysis specifically tailored to this configuration.

4.3 Distributed expression of the gradient

The shape derivative can be written in distributed form, as in Theorem 3 or in strong form (47), i.e., as a sum of integrals over the edges of the diagram, which only depend on θ and not on $D\theta$. In the context of free-form shape deformations, distributed expressions of shape derivatives may be advantageous due to their higher accuracy in the context of finite elements [30] and ease of implementation [38]. In the context of piecewise smooth shapes considered here, the advantage of the distributed shape derivative is that the higher regularity of S_1 required in Theorem 2 is not required. However, the term $D\theta$ appearing in (38) creates a difficulty, since θ is only known explicitly along the edges of the Voronoi diagram according to Theorem 1. This can be resolved in the case of Voronoi diagrams by extending θ inside the cells using a triangulation and piecewise linear function, as done in [14, Section 4.2]. Here we follow a similar idea, but we are facing the more general situation where a subset Ω_0 of $\mathcal{D}$ is not part of the Voronoi diagram. Compared to [14, Theorem 5] we obtain a slightly less explicit expression of $\nabla G(\mathbf{a})$, and we express $\nabla G(\mathbf{a})$ as a sum over the vertices of the Voronoi diagram, while in [14, Theorem 5] the sum is expressed as a double sum over the cells and the vertices of each cell.

Let $\mathcal{V}$ be the set of vertices of the Voronoi diagram $\mathbf{\Omega}(\mathbf{a})$. Since $\Omega_i(\mathbf{a})$, $i \in \mathcal{K}_{\mathrm{vor}}$, is convex, we can partition $\Omega_i(\mathbf{a})$ into a set of non-overlapping triangles, where the vertices of each triangle are the site a_i and two consecutive vertices of $\Omega_i(\mathbf{a})$, using a counterclockwise orientation. Let $\mathcal{D}_{\hat{\delta}}$ be the intermediate set defined in (27). We also partition $\Omega_0 \cap \mathcal{D}_{\hat{\delta}}$ into a set of non-overlapping triangles, where the vertices of each triangle are either in $\mathcal{V}$ or on $\partial\mathcal{D}_{\hat{\delta}}$. The union of these triangles thus forms a triangulation $\mathcal{T}$ of $\mathcal{D}_{\hat{\delta}}$. For $v \in \mathcal{V}$, introduce the basis functions $\psi_v \in C^0(\mathcal{D}_{\hat{\delta}}, \mathbb{R})$ such that $\psi_v(v) = 1$, $\psi_v(w) = 0$ for all other vertices w of the triangulation $\mathcal{T}$, and ψ_v is linear on each of the triangle in $\mathcal{T}$. Due to the continuity of ψ_v, this determines ψ_v uniquely in $\mathcal{D}$. The expression of ψ_v and $\nabla\psi_v$ can be computed explicitly on each $T \in \mathcal{T}$ for numerical purposes, see [14, Section 4.2]. We then have the following result.

Theorem 5. *Suppose Assumptions 2 and 3 hold, then the gradient of $G(\mathbf{a})$, defined in (16), is given by*

$$\nabla G(\mathbf{a}) \cdot \delta\mathbf{a} = \sum_{v \in \mathcal{V}^{int}} \delta a_{i_v} \cdot g^v_{i_v} + \delta a_{j_v} \cdot g^v_{j_v} + \delta a_{k_v} \cdot g^v_{k_v} + \sum_{v \in \mathcal{V}^{bd}} \delta a_{i_v} \cdot \mathfrak{g}^v_{i_v} + \delta a_{j_v} \cdot \mathfrak{g}^v_{j_v}, \tag{52}$$

where $\mathcal{V}^{int}$ is the set of interior vertices (w.r.t. $\mathcal{D}_0$) of the Voronoi diagram and $\mathcal{V}^{bd}$ the set of boundary vertices (w.r.t. $\mathcal{D}_0$), (i_v, j_v, k_v) are the indices of the three cells that share the common vertex $v \in \mathcal{V}^{int}$, i.e., $v = \overline{\Omega_{i_v}(\mathbf{a})} \cap \overline{\Omega_{j_v}(\mathbf{a})} \cap \overline{\Omega_{k_v}(\mathbf{a})}$, (i_v, j_v) are the indices of the two cells that share the common vertex $v \in \mathcal{V}^{bd}$, and, writing $(i, j, k) = (i_v, j_v, k_v)$ for simplicity,

$$\begin{aligned} g^v_i &:= M_v(j,k,i)^\top I(v), \quad g^v_j := M_v(k,i,j)^\top I(v), \quad g^v_k := M_v(i,j,k)^\top I(v), \\ \mathfrak{g}^v_i &:= \mathscr{M}^\ell_v(j,i)^\top I(v), \quad \mathfrak{g}^v_j := \mathscr{M}^\ell_v(i,j)^\top I(v). \end{aligned}$$

Here

$$M_v(i,j,k) := \frac{(a_i - a_j)^\perp \otimes (v - a_k)^\top}{Q(i,j,k)}, \qquad Q(i,j,k) := \det \begin{pmatrix} (a_j - a_i)^\top \\ (a_k - a_i)^\top \end{pmatrix} \tag{53}$$

and

$$\mathscr{M}^\ell_v(j,i) := \frac{-\nabla_x \varphi_\ell(v)^\perp \otimes (v - a_i)^\top}{\det \begin{pmatrix} (a_j - a_i)^\top \\ \nabla_x \varphi_\ell(v)^\top \end{pmatrix}} \tag{54}$$

where φ_ℓ is defined in Section 3.2. Also,

$$I(v) := \int_{supp(\psi_v)} S_1(\mathbf{\Omega}(\mathbf{a})) \nabla\psi_v(x) + S_0(\mathbf{\Omega}(\mathbf{a}))\psi_v(x)\, dx \tag{55}$$

where $supp(\psi_v) \subset \mathcal{D}$ is the support of ψ_v.

Proof. The proof is similar to the proof of [14, Theorem 5] and is provided in the appendix for convenience. □

Remark 4. *Once the triangulation $\mathcal{T}$ is chosen explicitly, a more explicit formula for the integral (55) can be computed for numerical purposes, as in [14].*

5 Conductivity problem with internal measurements

In the previous sections, we have presented the shape sensitivity analysis of the Voronoi diagram for EIT. Many of these developments apply directly or can be adapted in a straightforward manner to the case of the conductivity problem with internal data; see in particular Remark 1. Thus, we only present the main results here and we omit the proofs, which are similar to the EIT case.

We consider the inverse problem of determining a scalar-valued conductivity $\sigma^\star$ of a body $\mathcal{D} \subset \mathbb{R}^2$ satisfying the elliptic equation

$$\operatorname{div}(\sigma^\star \nabla U^\star) = f \text{ in } \mathcal{D}, \tag{56}$$

$$U^\star = 0 \text{ on } \partial\mathcal{D}, \tag{57}$$

from noisy domain measurements $h = U^\star|_{\mathcal{D}} + \eta$ of the ground truth potential $U^\star$ in $\mathcal{D}$, where $\eta : \mathcal{D} \to \mathbb{R}$ represents a measurement noise and $f \in H^1(\mathcal{D})$. The corresponding variational formulation is: Find $U^\star \in H^1_0(\mathcal{D})$ such that

$$\int_{\mathcal{D}} \sigma^\star \nabla U^\star \cdot \nabla W = \int_{\mathcal{D}} fW \quad \text{for all } W \in H^1_0(\mathcal{D}). \tag{58}$$

We consider a model conductivity $\sigma \in L^\infty(\mathcal{D})$ and the associated potential: Find $U \in H^1_0(\mathcal{D})$ such that

$$\int_{\mathcal{D}} \sigma \nabla U \cdot \nabla W = \int_{\mathcal{D}} fW \quad \text{for all } W \in H^1_0(\mathcal{D}). \tag{59}$$

The cost function is

$$J(\sigma) := \frac{1}{2} \int_{\mathcal{D}} (U(\sigma) - h)^2. \tag{60}$$

Unlike the EIT case, for this problem we assume $\mathcal{D}_0 = \mathcal{D}$ and we consider a similar setting where $\mathbf{\Omega}(\mathbf{a}) := \{\Omega_i(\mathbf{a})\}_{i \in \mathcal{K}_{\text{vor}}}$ is a Voronoi diagram with respect to $\mathcal{D}$, for a given $\mathcal{K}_{\text{vor}} = \{1, \dots, \kappa_0\}$. We assume that both $\sigma = \sigma_{\mathbf{\Omega}}$ and the ground truth $\sigma^\star$ are piecewise constant and have the form

$$\sigma_{\mathbf{\Omega}} := \sum_{i \in \mathcal{K}_{\text{vor}}} \sigma_i \chi_{\Omega_i}, \qquad \sigma^\star = \sum_{i \in \mathcal{K}_{\text{vor}}} \sigma_i \chi_{\Omega_i(\mathbf{a}^\star)},$$

where $\sigma_i, i \in \mathcal{K}_{\text{vor}}$ are given constants. As in the EIT problem, we define $\mathfrak{J}(\mathbf{\Omega}) := J(\sigma_{\mathbf{\Omega}})$ and the reduced cost functional

$$G(\mathbf{a}) := \mathfrak{J}(\mathbf{\Omega}(\mathbf{a})). \tag{61}$$

We have the following result for shape differentiability; we omit the proof, which is similar to the proof of Theorem 3. At this point, $\mathbf{\Omega} \in \mathbb{P}_{\mathcal{K}}(\mathcal{D})$ is a diagram in the sense of Definition 1, but not necessarily a Voronoi diagram.

Theorem 6 (distributed shape derivative)**.** *Assume $\mathbf{\Omega} \in \mathbb{P}_{\mathcal{K}}(\mathcal{D})$, $f \in H^1(\mathcal{D})$, $h \in H^1(\mathcal{D})$. Suppose the mapping T satisfies Assumption 1, then the shape derivative of $\mathcal{J}$ at $\mathbf{\Omega}$ in direction $\theta := \partial_t T(\cdot, 0) \in \mathcal{C}^{0,1}_{\partial\mathcal{D}}(\overline{\mathcal{D}}, \mathbb{R}^2)$ is given by*

$$d\mathcal{J}(\mathbf{\Omega})(\theta) = \int_{\mathcal{D}} S_1(\mathbf{\Omega}) : D\theta + S_0(\mathbf{\Omega}) \cdot \theta \, dx \tag{62}$$

where $S_1(\mathbf{\Omega}) \in L^1(\mathcal{D}, \mathbb{R}^{2\times 2})$ and $S_0(\mathbf{\Omega}) \in L^1(\mathcal{D}, \mathbb{R}^2)$ are defined by

$$S_1(\mathbf{\Omega}) = \left[\frac{1}{2}(U-h)^2 - fp + \sigma_{\mathbf{\Omega}} \nabla U \cdot \nabla p\right] I_2 - \sigma_{\mathbf{\Omega}} \nabla p \otimes \nabla U - \sigma_{\mathbf{\Omega}} \nabla U \otimes \nabla p, \tag{63}$$

$$S_0(\mathbf{\Omega}) = -(U-h)\nabla h - p \nabla f. \tag{64}$$

The adjoint $p \in H^1_0(\mathcal{D})$ is solution of

$$\int_{\mathcal{D}} \sigma_{\mathbf{\Omega}} \nabla p \cdot \nabla W = -\int_{\mathcal{D}} (U-h)W \quad \textit{for all } W \in H^1_0(\mathcal{D}). \tag{65}$$

We have the following higher regularity, which is proved similarly to Proposition 1.

Proposition 3. *Suppose the assumptions of Theorem 6 and Assumption 2 hold. Then* $S_1(\mathbf{\Omega}(\mathbf{a}))|_{\Omega_i(\mathbf{a})} \in W^{1,1}(\Omega_i(\mathbf{a}), \mathbb{R}^{2\times 2})$ *for all* $i \in \mathcal{K}_{vor}$.

Theorem 2 has been written for the EIT case, i.e., for $\delta > 0$. Nevertheless, it can be straightforwardly adapted to the case $\delta = 0$ and $\mathcal{D}_0 = \mathcal{D}$ needed here. Applying Theorem 2, Theorem 6 and Proposition 3, we get the following result.

Theorem 7. *Suppose the assumptions of Theorem 6 and Assumption 2 hold, then the gradient of* $G(\mathbf{a})$, *defined in* (61), *is given by*

$$\nabla G(\mathbf{a}) \cdot \delta\mathbf{a} = \sum_{i\in\mathcal{K}_{vor}} \sum_{E\in\mathcal{E}_i^{\text{int}}} \int_E (S_1(\mathbf{\Omega}(\mathbf{a}))\nu\cdot\nu)|_{\Omega_i(\mathbf{a})} \frac{(x-a_i)\cdot\delta a_i - (x-a_{k(i,E)})\cdot\delta a_{k(i,E)}}{\|a_{k(i,E)}-a_i\|}dx, \tag{66}$$

where $k(i,E)$ *is the index such that* $E = \overline{\Omega_i(\mathbf{a})} \cap \overline{\Omega_{k(i,E)}(\mathbf{a})}$ *and* $S_1(\mathbf{\Omega}(\mathbf{a}))$ *is given by* (63).

The expression of $\nabla G(\mathbf{a})$ may be simplified as follows. We omit the proof which is similar to the proof of Corollary 3.

Corollary 4. *Suppose the assumptions of Theorem 6 and Assumption 2 hold, then*

$$\nabla G(\mathbf{a}) \cdot \delta\mathbf{a} = \sum_{i\in\mathcal{K}_{vor}} \sum_{E\in\mathcal{E}_i^{\text{int}}} \delta a_{k(i,E)} \cdot \lambda_{k,E} + \delta a_i \cdot \lambda_{i,E}, \tag{67}$$

with

$$\lambda_{k,E} = -\int_E \mathfrak{S}_i \frac{(x-a_{k(i,E)})}{\|a_{k(i,E)}-a_i\|}dx, \qquad \lambda_{i,E} = \int_E \mathfrak{S}_i \frac{(x-a_i)}{\|a_{k(i,E)}-a_i\|}dx$$

and $\mathfrak{S}_i := \sigma_i(\nabla U\cdot\nabla p - 2\partial_\nu p\partial_\nu U)|_{\Omega_i(\mathbf{a})}$.

Summarizing, the results for the conductivity problem with internal measurements are similar to EIT as the analysis of the weak singularities is performed in the same way, see Section 4.1. The main differences are that only a single measurement is involved here, and that $\mathcal{D}_0 = \mathcal{D}$, meaning some cells of the Voronoi diagram are in contact with the boundary $\partial\mathcal{D}$.

6 Numerical experiments

In this section, we report numerical experiments with the two problems considered in this work: the EIT problem (inverse conductivity problems with boundary measurements) and the inverse conductivity problem with internal measurements. The experiments begin by evaluating the performance of the Spectral Projected Gradient [15] method in the optimization process (Section 6.1). We then evaluate the usefulness of a multistart strategy in the optimization process (Section 6.2), using instances of the inverse conductivity problem with internal measurements, $\kappa_0 \in \{5, 6, \ldots, 14\}$ and equidistant $\sigma^\star$. In the sequel (Section 6.3), we consider instances of the inverse problem with boundary measurements (EIT) with increasing noise and with single and multiple measurements.

In [14, Section 5.2], a detailed comparison of the interface and distributed expressions of the gradient has been conducted for the potential problem. The advantages and disadvantages of both approaches have been discussed—for example, the fact that the numerical computation of integrals over triangles is simpler for the distributed expression compared to computing interface integrals for the interface expression. The numerical results in [14, Section 5.2] indicate that the reconstructions are similar for all considered experiments. Additionally, the optimization method requires approximately the same number of iterations and function evaluations per iteration for both gradient formulations. However, the computation of the interface expression is three times faster than that of the distributed expression. Since we expect a similar behavior for the conductivity problems studied in this paper, we have chosen to use the interface expression of the gradient exclusively.

In the experiments, we constructed problems with known solution $\sigma^\star$ for different values of κ_0. The construction starts by choosing κ_0 and drawing $a_i^\star \in \mathcal{D} = (0,1)\times(0,1)$ for all $i \in \mathcal{K}_{\text{vor}} = \{1,\dots,\kappa_0\}$. Then we set $\sigma_i^\star = i$ for all $i \in \mathcal{K}_{\text{vor}}$. We call this case equidistant. Additional scenarios where each $\sigma_i^\star$ is randomly assigned a value in $\{5,10\}$ (binary case) or a value in $\{3,6,9\}$ (ternary case) are also considered. Results with instances in these simpler scenarios have been performed and are mentioned in the following sections. However, due to space limitations, only numerical experiments with the equidistant case are fully reported.

In all the reported experiments, the initial points were generated as perturbations of the ground truth. Completely random initial points were also tested, but the results were unsatisfactory and are not included here. Note that initializations based on ground truth perturbations are not unrealistic in real-world scenarios. In practice, a sequence of methods and heuristics are often used to obtain reconstructions, and the ground truth perturbation typically reflects the outcome of another method that provides a rough first approximation, without requiring prior knowledge. This is well exemplified by topological derivative-based approaches, such as [16, 28, 29], which on one hand do not require prior knowledge of the ground truth but on the other hand are not designed to provide a precise approximation of the interfaces.

In the EIT problem, we also take $\sigma_0 = 1$ in the boundary layer Ω_0. Then we choose $\Gamma_a = \Gamma_{\text{upper}}\cup\Gamma_{\text{lower}}$ and $\Gamma_b = \Gamma_{\text{left}}\cup\Gamma_{\text{right}}$, with $\Gamma_{\text{upper}} = \{x=(x_1,x_2)^T \in \overline{\mathcal{D}} \ : \ x_2 = 1\}$, $\Gamma_{\text{lower}} = \{x=(x_1,x_2)^T \in \overline{\mathcal{D}} \ : \ x_2 = 0\}$, $\Gamma_{\text{left}} = \{x=(x_1,x_2)^T \in \overline{\mathcal{D}} \ : \ x_1 = 0\}$, and $\Gamma_{\text{right}} = \{x=(x_1,x_2)^T \in \overline{\mathcal{D}} \ : \ x_1 = 1\}$. For the inverse conductivity problems with boundary measurements (EIT) we consider $\bar\alpha \in \{1,3\}$ and

$$\begin{array}{rclcrcl} g_1 &=& 1 \text{ on } \Gamma_{\text{left}}\cup\Gamma_{\text{right}} & \text{and} & g_1 &=& -1 \text{ on } \Gamma_{\text{upper}}\cup\Gamma_{\text{lower}},\\ g_2 &=& 1 \text{ on } \Gamma_{\text{left}}\cup\Gamma_{\text{upper}} & \text{and} & g_2 &=& -1 \text{ on } \Gamma_{\text{right}}\cup\Gamma_{\text{lower}},\\ g_3 &=& 1 \text{ on } \Gamma_{\text{left}}\cup\Gamma_{\text{lower}} & \text{and} & g_3 &=& -1 \text{ on } \Gamma_{\text{right}}\cup\Gamma_{\text{upper}}. \end{array}$$

When $\bar\alpha = 1$, only g_1 is used, while when $\bar\alpha = 3$, g_1, g_2 and g_3 are used. Then, we solve (3,4) to obtain $U_\alpha^\star$ for $\alpha = 1,\dots,\bar\alpha$. Synthetic measurements h_α are obtained via the formula $h_\alpha := U_\alpha^\star + \eta_\alpha$, where η_α is a normal Gaussian noise with mean zero and standard deviation $c\|u_\alpha^\star\|_\infty$ and c is a parameter that takes different values depending on the experiment. For the inverse conductivity problem with internal measurements, we set $f \equiv 1$ and $h := U^\star + \eta$.

In the generated instances, $a_i^\star \in \mathcal{D}$ for $i \in \mathcal{K}_{\text{vor}}$. Including this information in the problem (17), we arrive at the bound constrained minimization problem given by

$$\underset{\mathbf{a}\in\mathbb{R}^{2\kappa_0}}{\text{Minimize}}\, G(\mathbf{a}) \text{ subject to } \mathbf{a} \in \overline{\mathcal{D}}. \tag{68}$$

When the problem (68) refers to the EIT problem, the objective function G is defined in (16). Therefore, the evaluation of G needs the evaluation of $\mathfrak{J}$ defined in (15) which, in turn, needs the calculation of U_α and V_α, solutions of (6) and (7), respectively. The expression for ∇G is given in (48). When the above problem refers to the inverse conductivity problem with internal measurements, the expression of G is given by (61), with $\mathfrak{J}(\mathbf{\Omega}(\mathbf{a})) = J(\sigma_{\mathbf{\Omega}(\mathbf{a})})$, $J(\sigma)$ defined in (60), with $U(\sigma)$ solution of (59). For practical purposes we consider an additional weight in the cost function, i.e.,

$$J(\sigma) := \frac{\zeta}{2}\int_{\mathcal{D}} (U(\sigma)-h)^2. \tag{69}$$

In this case, ∇G is given by (67), multiplied by the weight ζ. The calculations of $G(\mathbf{a})$ and $\nabla G(\mathbf{a})$ require the calculation of a Voronoi diagram associated with the sites $\mathbf{a}$. For this calculation we use the routines introduced in [11, 12, 13].

In the inverse conductivity problems with boundary and internal measurements, the values of ζ_α for $\alpha = 1,\dots,\bar\alpha$ in the definition of $G(\mathbf{a})$ and ζ in (69) are computed in practice as

$$\zeta_\alpha = \frac{1}{\displaystyle\int_{\mathcal{D}} (U_\alpha(\sigma_{\mathbf{\Omega}(\mathbf{a}^0)}) - V_\alpha(\sigma_{\mathbf{\Omega}(\mathbf{a}^0)}))^2} \ \text{ and } \ \zeta = \frac{1}{\displaystyle\int_{\mathcal{D}} (U(\sigma_{\mathbf{\Omega}(\mathbf{a}^0)}) - h)^2},$$

respectively, where $\mathbf{a}^0$ is the initial guess of the optimization process. In this way, the terms corresponding to each measurement h_α start with the same magnitude in the calculation of G. (As a consequence,

$G(\mathbf{a}^0) = \bar{\alpha}/2$ for EIT and $G(\mathbf{a}^0) = 1/2$ for internal measurements). The noise level of the generated instance is then computed as

$$\text{Noise} = 100\% \times \sqrt{\frac{\sum_{\alpha=1}^{\bar{\alpha}} \zeta_\alpha \|h_\alpha - U_\alpha^\star\|^2_{L^2(\partial\mathcal{D})}}{\sum_{\alpha=1}^{\bar{\alpha}} \zeta_\alpha \|U_\alpha^\star\|^2_{L^2(\partial\mathcal{D})}}} \quad \text{and} \quad \text{Noise} = 100\% \times \frac{\|h - U^\star\|_{L^2(\mathcal{D})}}{\|U^\star\|_{L^2(\mathcal{D})}} \tag{70}$$

in the inverse conductivity problems with boundary measurement (EIT) and internal measurement, respectively.

Given an approximation $\hat{\mathbf{a}}$ of a solution to an instance with known solution $\sigma^\star$, in the following sections we refer to the error $E(\hat{\mathbf{a}})$ of $\hat{\mathbf{a}}$ defined as

$$E(\hat{\mathbf{a}}) = 100\% \times \frac{\displaystyle\int_{\mathcal{D}} |\sigma^\star - \sigma(\hat{\mathbf{a}})|}{\displaystyle\int_{\mathcal{D}} \sigma^\star}. \tag{71}$$

In [14], we used the Projected Gradient (PG) method [10, 22, 39] in the optimization process. However, in practice, numerical inaccuracies in the computation of the objective function prevent the method from recognizing, at each iteration, that a tentative point satisfies a certain condition of decrease of the objective function with respect to the current point. In the experiments of this work, we verify whether a non-monotone linear search such as that of the Spectral Projected Gradient (SPG) method [15] can be beneficial in such a scenario. In the SPG non-monotone linear search, at each iteration a decrease of the objective function is required, not relative to the current iterate, but to the maximum of the last M iterations, where $M > 0$ is a given constant. Thus, the sequence of function values generated by the method is not necessarily monotonically decreasing. Let $\mathbf{a}^0, \mathbf{a}^1, \mathbf{a}^2, \ldots$ be the sequence of iterates generated by the optimization method. As a stopping criterion we consider $\|\mathbf{a}^\ell - \mathbf{a}^{\ell-1}\|_\infty \leq \epsilon$, with $\epsilon = 10^{-6}$, which corresponds to lack of progress. We would like to have used a stopping criterion asking for a small $\nabla G(\mathbf{a}^\ell)$, but as its calculation depends on the numerical resolution of one or two PDEs, it is difficult to obtain small values in practice. Precisely, the lack of progress is a consequence of the error in the calculations of G and ∇G.

We implemented PG and SPG within the computing platform FEniCS [35, 40], an open-source software for solving PDEs with the finite element method. The domain $\mathcal{D}$ was discretized using a regular grid with 128 cells in each direction and crossed diagonals. The function spaces used in the experiments were built using standard Lagrange finite elements: piecewise linear elements (P1) and piecewise quadratic elements (P2). The P2 elements were used to compute $\mathcal{H}$, whereas the other functions such as U, V, p, q were approximated using P1 elements. The Neumann problem (3)-(4) for the ground truth $U_\alpha^\star$ was solved using a mixed function space combining P1 elements and a real-valued Lagrange multiplier to deal with the compatibility condition (2) and the vanishing integral mean. Regarding the numerical solution of the resulting linear systems, FEniCS uses sparse LU decomposition by default. The SPG method, as described in [15], has only a few parameters. The parameter $M \geq 1$ defines the degree of non-monotonicity of the sequence of objective function values generated by the method. In the experiments of the next section, we considered $M = 3$ and $M = 5$. The parameters $0 < \lambda_{\min} \leq \lambda_{\max}$ define the safeguards for the spectral step. As recommended in [15], we considered $\lambda_{\min} = 10^{-16}$ and $\lambda_{\max} = 10^{16}$. The line search has the parameter $\gamma > 0$ of the non-monotone Armijo descent condition, whose usual value in the literature is $\gamma = 10^{-4}$. We used this value in our experiments. In the line search, each trial step α uses safeguards $0 < \sigma_1 \leq \sigma_2 < 1$ such that a trial step α is between σ_1 times the previous trial and σ_2 times the previous trial. As usual in the literature, we considered $\sigma_1 = 0.1$ and $\sigma_2 = 0.9$. To allow full reproducibility, the codes are available at `https://github.com/Souza-DR/bls2024-conductivity`.

6.1 Performance evaluation of a non-monotone optimization process

In this section we consider four instances of the inverse conductivity problem with internal data with $\kappa_0 \in \{5, 6, 7, 8\}$ and equidistant $\sigma^\star$. In the definition of h, we consider parameter $c = 0.02$ in the noise generation. We solved each of the four instances using the PG method and SPG method with $M \in \{3, 5\}$. Table 1 shows the results. In the table, we show the noise of each instance, the error,

the objective function value, and the gradient norm of the initial and final reconstructions, and three measures of the optimization process cost: the number of iterations, the number of functional evaluations and the CPU time in seconds. The figures in the table show that the PG method performed, in average, 37.25 iterations per problem, 5.66 function evaluations per iteration and took about 0.95 seconds for each functional evaluation. These figures are 56.75, 2.84 and 0.79 for the SPG with $M = 3$ and 131.25, 2.56 and 0.78 for the SPG with $M = 5$. As expected, the more relaxed criteria for the acceptance of the new iterate reduces by half the number of function evaluations per iteration, when we compare the PG method with the SPG method (both with $M = 3$ and $M = 5$). On the other hand, the SPG method uses a larger number of iterations than the PG method. This higher number of iterations is not compensated by the reduction in the number of function evaluations per iteration and, thus, the SPG takes longer than the PG method. This is compensated by the fact that the SPG method with $M = 5$ found final reconstructions with lower values of the objective function in 3 out of the 4 cases. In the remainder of this paper, we will consider the SPG with $M = 5$ for all optimization processes.

	κ_0	Noise	$E(\mathbf{a}^0)$	$E(\hat{\mathbf{a}})$	$G(\mathbf{a}^0)$	$G(\hat{\mathbf{a}})$	$\|\nabla G(\mathbf{a}^0)\|_2$	$\|\nabla G(\hat{\mathbf{a}})\|_2$	#iter	#feval	Time
PG	5	2.32	13.84	3.40	0.50	0.02645	1.57395	0.03734	33	153	176.25
	6	3.03	9.23	1.46	0.50	0.08382	0.99416	0.14532	23	146	176.85
	7	2.47	14.67	2.77	0.50	0.02769	1.42491	0.01772	71	404	543.72
	8	3.22	9.71	2.91	0.50	0.07477	1.39102	0.11703	22	131	189.81
SPG $M = 3$	5	2.32	13.84	2.78	0.50	0.02549	1.57395	0.01956	27	78	93.53
	6	3.03	9.23	1.74	0.50	0.08650	0.99416	0.04638	40	115	148.32
	7	2.47	14.67	3.04	0.50	0.02802	1.42491	0.01060	113	292	408.04
	8	3.22	9.71	3.01	0.50	0.07569	1.39102	0.12099	47	141	209.88
SPG $M = 5$	5	2.32	13.84	1.92	0.50	0.02445	1.57395	0.00301	225	505	624.42
	6	3.03	9.23	0.73	0.50	0.08030	0.99416	0.00720	152	411	535.19
	7	2.47	14.67	2.87	0.50	0.02778	1.42491	0.02568	112	280	397.19
	8	3.22	9.71	2.64	0.50	0.07059	1.39102	0.05199	36	101	160.01

Table 1: Synthetic comparison of the optimization process performed with the Projected Gradient (PG) method and with the Spectral Projected Gradient (SPG) method with non-monotonicity parameter $M \in \{3, 5\}$.

6.2 Usefulness of a multistart strategy in the optimization process

In this section, we consider the same four instances of the previous section, i.e., four instances of the inverse conductivity problem with internal data, $\kappa_0 \in \{5, 6, 7, 8\}$, and equidistant $\sigma^\star$, plus six additional instances with the same characteristics but $\kappa_0 \in \{9, 10, 11, 12, 13, 14\}$. We solved those ten instances with the SPG method with $M = 5$ using ten different initial points generated as ground truth perturbations. This means the initial estimation is given by $a_i^0 = a_i^\star + r$, where r is a random number with uniform distribution in $[-0.1, 0.1]$, for all $i \in \mathcal{K}_{\text{vor}}$. Tables 2, 3 and 4 show the results. In Table 2, the first line for each value of $\kappa_0 \leq 8$ corresponds exactly to what was presented in Table 1 for the SPG with $M = 5$. Tables 2, 3 and 4 show an additional last column compared to Table 1. This column corresponds to the value of $G_{\zeta \equiv 1}$ at the final reconstruction $\hat{\mathbf{a}}$. As mentioned at the beginning of the section, the function G is scaled by including in its definition the weight ζ (or the weights ζ_α for $\alpha = 1, \ldots, \bar{\alpha}$ in the case of the EIT problem), which depends on $\mathbf{a}^0$. This scaling implies that $G(\mathbf{a}^0) = \frac{1}{2}\bar{\alpha}$. For this reason, values of $G(\hat{\mathbf{a}})$ obtained using different initial points $\mathbf{a}^0$ cannot be directly compared. $G_{\zeta \equiv 1}$ corresponds to the function G with $\zeta_\alpha = 1$ for $\alpha = 1, \ldots, \bar{\alpha}$. The values of $G_{\zeta \equiv 1}(\hat{\mathbf{a}})$ for different approximate solutions $\hat{\mathbf{a}}$ can be compared with the belief that the smaller the better. In that column, for each instance, the smallest value of $G_{\zeta \equiv 1}(\hat{\mathbf{a}})$ is shown in bold. What is noteworthy is that this smallest value of $G_{\zeta \equiv 1}(\hat{\mathbf{a}})$ corresponds, in nine of the ten cases to the smallest or second-smallest value of $E(\hat{\mathbf{a}})$ and in only one case to the third-smallest value. This relationship justifies the choice of the final reconstruction with the smallest value of $G_{\zeta \equiv 1}(\hat{\mathbf{a}})$ as solution for a given instance. Of course, choosing the solution $\hat{\mathbf{a}}$ with the smallest $E(\hat{\mathbf{a}})$ should be easier, but computing $E(\hat{\mathbf{a}})$ requires acknowledging the ground truth, which is generally not available.

Figures 3, 4, and 5 show the graphical representation of the solutions chosen in this way. The

reconstructions are visually quite accurate, especially for smaller values of κ_0. The most significant aspect, qualitatively, is that the algorithm successfully captures most of the topological features of the ground truth. For instance, in the case $\kappa_0 = 9$ shown in Figure 4, the reconstruction preserves exactly the same topological characteristics as the ground truth: the cells have the same number of edges and are connected to their neighboring cells in the same manner. In contrast, the topological features of the initialization are more notably altered; compare, for example, the groups of cells with indices $\{1, 2, 3\}$ and $\{4, 6, 9\}$. However, it is worth noting that, given the ill-posed nature of the problem, the initialization was taken not too far off from the ground truth in terms of spatial arrangement, in the sense that the cells in the initialization occupy positions similar to those in the ground truth.

Naturally, the greater the number of random initial points considered, the better the quality of the final reconstruction. We chose to keep this number at ten in order to keep the total cost of the experiments moderate. It is worth noting that with this strategy we found for all ten instances solutions $\hat{\mathbf{a}}$ with average $E(\hat{\mathbf{a}})$ equal to 2.03% and never greater than 3.76%. On the other hand, each optimization process starting from a different initial point is independent of the others and this process can easily benefit from a parallel computing environment. Experiments analogous to those reported in this section were also performed with binary and ternary ground truths. The results obtained were analogous, and these experiments were not included in the present work, since the binary and ternary cases are expected to be simpler than the equidistant case presented here.

6.3 EIT with different noise levels using single and multiple measurements

In this section we consider instances of the inverse conductivity problem with boundary measurements (EIT), $\kappa_0 \in \{5, 6, 7, 8, 9\}$, equidistant $\sigma_i^\star$ and four noise levels with $c \in \{0.0, 0.0025, 0.005, 0.01\}$. We start with the case $\bar{\alpha} = 1$. In all the cases with $\kappa_0 \leq 8$, solutions $\hat{\mathbf{a}}$ with $E(\hat{\mathbf{a}})$ less than or equal to 5% were found. On the other hand, as shown in Table 5 and Figure 6, for the case $\kappa_0 = 9$, a solution $\hat{\mathbf{a}}$ with $E(\hat{\mathbf{a}})$ less than or equal to 5% was found only for the noiseless instance. Therefore, in the sequence, we consider the instance with $\kappa_0 = 9$ and different noise levels with $\bar{\alpha} = 3$ measurements. Table 6 and Figure 7 show the results. We observe that, considering $\bar{\alpha} = 3$ measurements, $\hat{\mathbf{a}}$ with $E(\hat{\mathbf{a}})$ less than or equal to 5% were found in all four cases. It should be noted that, with more measurements, the evaluation of the objective function and its gradient is computationally more expensive. In almost all cases, the optimization process reached a time limit of four hours of CPU time. Even so, the objective function is reduced by about two orders of magnitude. As in the case of internal measurements (see the discussion in Section 6.2), the algorithm is able to successfully captures most of the topological features of the ground truth, whereas the topological features of the initialization are altered. We observe some small differences between the topological features of the reconstruction and the ground truth, see for instance the configuration of cells $\{1, 8, 9\}$ in the case $\kappa_0 = 9$ and $c = 0.005$ of Figure 6.

To conclude, two key points are worth noting here. First, EIT is inherently more challenging than the problem with internal measurements, as it relies solely on boundary measurements, which naturally results in lower reconstruction quality. Second, only a single measurement was used to produce the results in Figure 6, which is a challenging problem considering the complexity of the geometry. Indeed, uniqueness of the reconstruction with a single measurement has only been proven for much simpler geometries, see for instance [6, 21].

7 Concluding remarks

In [14] we have investigated the reconstruction of the potential coefficient in an elliptic equation that is piecewise constant on a Voronoi diagram. Here we have extended this investigation to the case of conductivity coefficients in elliptic equations, with applications to EIT. The solution of the PDE in the conductivity case exhibits strong singularities at the vertices of the Voronoi diagram, which must be carefully analyzed to prove the shape differentiability. An important aspect of both [14] and the present work is the relation between the distributed and the boundary expression of the shape gradients, which leads to two different formulas of the cost functional gradient and consequently to two possible numerical implementations. On the one hand, the advantage of the distributed expression, which involves volumetric integrals, is that the shape tensors $S_1(\boldsymbol{\Omega})$ and $S_0(\boldsymbol{\Omega})$ in Theorems 3 and 6 do not need a regularity analysis and can be used directly in a numerical implementation. This means that the analysis

κ_0	Noise	$E(\mathbf{a}^0)$	$E(\hat{\mathbf{a}})$	$G(\mathbf{a}^0)$	$G(\hat{\mathbf{a}})$	$\|\nabla G(\mathbf{a}^0)\|_2$	$\|\nabla G(\hat{\mathbf{a}})\|_2$	#iter	#feval	Time	$G_{\varsigma\equiv 1}(\hat{\mathbf{a}})$
5	2.32	13.84	1.92	0.50	0.02445	1.57395	0.00301	225	505	626.46	8.789e-08
5	2.32	9.87	2.36	0.50	0.03955	1.81973	0.03055	80	228	809.44	8.820e-08
5	2.32	8.27	2.02	0.50	0.08871	1.92878	0.01568	70	152	668.40	8.755e-08
5	2.32	12.43	0.93	0.50	0.01679	1.60892	0.00382	63	154	622.87	8.700e-08
5	**2.32**	**13.27**	**1.25**	**0.50**	**0.02127**	**1.90923**	**0.00297**	**211**	**548**	**2209.45**	**8.685e-08**
5	2.32	3.35	9.51	0.50	0.26747	1.79383	0.66214	159	522	1705.58	1.648e-07
5	2.32	6.02	1.83	0.50	0.09077	1.94004	0.01131	105	246	1153.10	8.781e-08
5	2.32	14.40	2.22	0.50	0.01287	1.61256	0.00159	60	153	680.89	8.806e-08
5	2.32	5.34	1.30	0.50	0.10172	1.83832	0.03547	50	148	597.60	8.818e-08
5	2.32	10.60	3.14	0.50	0.13292	1.88523	0.05744	41	115	488.08	9.029e-08
6	3.03	9.23	0.73	0.50	0.08030	0.99416	0.00720	152	411	556.57	1.003e-07
6	3.03	8.60	0.52	0.50	0.04922	1.40413	0.02770	43	119	574.56	9.897e-08
6	3.03	14.21	0.74	0.50	0.02369	1.29775	0.00825	55	133	716.46	1.008e-07
6	3.03	14.99	1.67	0.50	0.03576	0.70385	0.01571	98	227	1287.84	1.123e-07
6	3.03	10.42	0.45	0.50	0.03570	0.69982	0.00610	95	235	1291.99	9.935e-08
6	3.03	5.20	0.62	0.50	0.05205	2.19807	0.00928	94	235	1304.52	9.917e-08
6	3.03	11.85	0.69	0.50	0.02388	1.89691	0.00530	106	262	1503.37	1.003e-07
6	**3.03**	**9.30**	**0.36**	**0.50**	**0.08260**	**1.09238**	**0.00667**	**88**	**225**	**1280.05**	**9.892e-08**
6	3.03	10.22	0.89	0.50	0.04079	0.90450	0.03334	54	131	790.94	1.015e-07
6	3.03	16.19	0.88	0.50	0.01783	1.65585	0.00361	140	318	2058.18	1.014e-07
7	2.47	14.67	2.87	0.50	0.02778	1.42491	0.02568	112	280	406.58	4.057e-08
7	2.47	8.67	2.65	0.50	0.11333	1.50008	0.03911	87	205	1557.46	3.987e-08
7	2.47	8.26	2.41	0.50	0.07235	1.87241	0.03682	156	379	2858.96	3.846e-08
7	**2.47**	**11.52**	**1.29**	**0.50**	**0.03958**	**2.23856**	**0.01809**	**159**	**349**	**2939.70**	**3.799e-08**
7	2.47	7.15	2.23	0.50	0.15238	2.29956	0.07509	224	540	4309.49	3.891e-08
7	2.47	9.39	3.56	0.50	0.04344	1.64397	0.01005	108	306	2185.86	3.951e-08
7	2.47	6.26	1.87	0.50	0.05683	1.70631	0.02648	88	217	1745.32	3.967e-08
7	2.47	9.54	1.78	0.50	0.02788	1.40489	0.00655	111	271	2244.18	3.806e-08
7	2.47	12.91	1.90	0.50	0.15814	1.96233	0.01145	137	335	2815.65	3.813e-08
7	2.47	9.72	1.88	0.50	0.03994	2.15260	0.01390	110	300	2320.54	3.804e-08
8	3.22	9.71	2.64	0.50	0.07059	1.39102	0.05199	36	101	154.64	8.492e-08
8	3.22	6.53	0.87	0.50	0.05853	0.92047	0.01241	157	353	3814.92	7.422e-08
8	3.22	9.05	1.86	0.50	0.10167	1.87974	0.03412	121	292	3025.71	7.591e-08
8	3.22	10.76	0.84	0.50	0.10036	1.37828	0.02507	133	337	3430.74	7.368e-08
8	3.22	10.79	1.10	0.50	0.04690	1.45101	0.01175	166	387	4287.64	7.485e-08
8	**3.22**	**7.10**	**0.78**	**0.50**	**0.06878**	**2.12588**	**0.00741**	**112**	**265**	**2962.12**	**7.358e-08**
8	3.22	9.76	0.83	0.50	0.07668	1.73118	0.02337	122	302	3283.14	7.388e-08
8	3.22	10.90	1.12	0.50	0.02822	2.01323	0.00849	119	281	3235.42	7.428e-08
8	3.22	8.53	0.67	0.50	0.04003	1.03357	0.00462	125	294	3450.71	7.363e-08
8	3.22	10.00	0.87	0.50	0.04068	1.09810	0.02049	66	164	1856.91	7.440e-08

Table 2: Results of using ten different initial points in the process of optimizing instances of the conductivity problem with internal measurements, $\kappa_0 \in \{5, 6, 7, 8\}$, and equidistant $\sigma^\star$.

and the numerical implementation are relatively easy to adapt if one changes the underlying PDE; one essentially needs to recompute the corresponding $S_1(\mathbf{\Omega})$ and $S_0(\mathbf{\Omega})$. On the other hand, the existence of a boundary expression involving integrals at the edges of the Voronoi diagram, requires a detailed analysis of the regularity of the solution of the underlying PDE. This regularity can vary significantly depending on the type of PDE and the specific parameter to be reconstructed. In particular, in the conductivity case this analysis is more complex compared to the potential case [14]. Related to this issue, it was also necessary to generalize the framework of [14] by introducing a boundary layer to avoid the lack of regularity of solutions on the boundary of $\mathcal{D}$. In [14], we observed that the numerical computation of the boundary gradient is three times faster than the computation of the distributed gradient, for the same results, which shows that the additional analysis required to obtain the boundary expression can be useful for the numerical realization. Considering these previous results, we have opted to use only the interface expression of the gradient for conductivity problems.

From an optimization point of view, the problems considered in this paper are challenging in many ways. They present many local non-global minimizers, the objective function is computationally ex-

κ_0	Noise	$E(\mathbf{a}^0)$	$E(\hat{\mathbf{a}})$	$G(\mathbf{a}^0)$	$G(\hat{\mathbf{a}})$	$\|\nabla G(\mathbf{a}^0)\|_2$	$\|\nabla G(\hat{\mathbf{a}})\|_2$	#iter	#feval	Time	$G_{\zeta\equiv 1}(\hat{\mathbf{a}})$
9	3.05	20.69	10.42	0.50	0.08061	1.59456	0.19981	11	43	69.66	1.109e-07
9	3.05	14.11	1.74	0.50	0.05866	1.63884	0.03365	176	431	5722.41	4.175e-08
9	3.05	18.53	10.55	0.50	0.13269	1.37553	0.93506	17	57	619.71	1.796e-07
9	3.05	17.75	7.38	0.50	0.02748	1.19211	0.12002	230	526	7675.06	5.187e-08
9	**3.05**	**12.38**	**1.64**	**0.50**	**0.04320**	**1.57088**	**0.01446**	**125**	**295**	**4283.45**	**4.134e-08**
9	3.05	12.37	2.43	0.50	0.06234	1.73905	0.01879	169	423	5932.15	4.264e-08
9	3.05	13.85	3.53	0.50	0.05248	1.61066	0.06157	120	276	4292.42	4.880e-08
9	3.05	17.78	18.69	0.50	0.08420	1.84086	0.17109	42	123	1741.63	3.078e-07
9	3.05	17.84	9.01	0.50	0.06722	1.72205	0.16450	46	119	1758.55	1.970e-07
9	3.05	13.98	14.29	0.50	0.12998	1.04280	0.20469	114	291	4471.82	9.273e-08
10	2.69	30.06	20.19	0.50	0.04767	1.13143	0.05833	47	150	255.85	1.265e-07
10	2.69	17.52	10.43	0.50	0.06197	1.82301	0.11740	187	435	8710.94	4.718e-08
10	2.69	18.28	5.64	0.50	0.02877	1.72603	0.07920	87	225	4264.91	2.679e-08
10	2.69	33.52	15.57	0.50	0.05601	1.23234	0.08386	79	212	4167.45	1.421e-07
10	2.69	19.27	19.78	0.50	0.04194	1.72884	0.09039	37	105	1945.40	7.415e-08
10	2.69	20.97	6.28	0.50	0.02580	1.72048	0.12663	88	228	4666.56	3.616e-08
10	**2.69**	**20.79**	**2.08**	**0.50**	**0.01828**	**1.76763**	**0.00966**	**314**	**748**	**16482.42**	**2.189e-08**
10	2.69	14.50	4.33	0.50	0.03339	1.77251	0.02499	134	320	7340.65	2.420e-08
10	2.69	11.65	3.59	0.50	0.10777	1.53868	0.10470	283	670	15906.48	2.527e-08
11	3.10	20.61	16.03	0.50	0.05048	1.66585	0.05891	100	231	440.81	8.346e-08
11	3.10	25.91	19.03	0.50	0.07569	2.07564	0.14712	126	290	8345.51	1.900e-07
11	3.10	22.35	3.81	0.50	0.04970	1.76190	0.01029	174	387	11309.82	5.078e-08
11	3.10	16.14	10.87	0.50	0.05196	1.77382	0.04083	86	227	5980.53	1.547e-07
11	3.10	18.46	4.32	0.50	0.03913	1.73745	0.01434	222	491	14951.01	5.084e-08
11	3.10	22.74	4.08	0.50	0.04322	1.75091	0.00949	171	402	11837.77	5.008e-08
11	**3.10**	**12.84**	**2.90**	**0.50**	**0.03615**	**1.56743**	**0.01055**	**69**	**198**	**4937.83**	**4.945e-08**
11	3.10	19.94	6.78	0.50	0.13705	1.68287	0.05164	77	181	5486.65	6.870e-08
11	3.10	13.79	2.84	0.50	0.04927	1.65762	0.02551	156	360	11257.69	5.019e-08
11	3.10	13.98	13.35	0.50	0.09788	1.31820	0.33009	18	79	1376.19	1.704e-07
12	2.98	18.49	2.04	0.50	0.03522	1.82255	0.01638	125	286	570.41	3.199e-08
12	2.98	15.33	7.97	0.50	0.02693	1.27821	0.05275	36	92	3008.83	4.153e-08
12	2.98	16.93	3.62	0.50	0.03133	1.95410	0.02426	171	390	13800.89	3.398e-08
12	2.98	11.61	5.13	0.50	0.07889	1.73299	0.05346	65	194	5445.55	3.874e-08
12	2.98	17.27	2.89	0.50	0.02405	1.40865	0.02112	71	183	5911.34	3.039e-08
12	2.98	18.77	9.24	0.50	0.04445	1.38472	0.05084	51	139	4290.87	6.926e-08
12	**2.98**	**16.13**	**2.76**	**0.50**	**0.05464**	**1.75073**	**0.00882**	**112**	**241**	**9433.72**	**3.019e-08**
12	2.98	15.60	4.86	0.50	0.03918	1.70271	0.04309	121	281	10804.14	3.384e-08
12	2.98	19.94	4.04	0.50	0.03623	1.62085	0.03217	84	201	7301.44	3.649e-08
12	2.98	15.22	5.91	0.50	0.05721	2.16036	0.17645	38	97	3466.54	4.776e-08

Table 3: Results of using ten different initial points in the process of optimizing instances of the conductivity problem with internal measurements, $\kappa_0 \in \{9, 10, 11, 12\}$, and equidistant $\sigma^\star$.

pensive to evaluate, as is its gradient, and the objective function and gradient are computed with error since they depend on the numerical solution of PDEs. In this paper, we showed that the problem of multiple local solutions can be partially circumvented by using different initial guesses. However, the initial guesses considered are perturbations of a known solution, and the study of alternative strategies could be a future line of work. In contrast to what was done in [14], in this paper we considered the use of the Spectral Projected Gradient (SPG) as an alternative to the classical Projected Gradient method. Equipped with a non-monotone linear search that allows the value of the objective function to be increased from one iteration to the next, SPG proved to be effective and generally found better quality solutions than the classical Projected Gradient. However, there are specialized methods for dealing with problems where the objective function and constraints are evaluated inaccurately. Checking whether the problems under consideration fit into the theoretical framework of these methods and whether they can be applied to them could also be a line of future work.

Conflict of interest statement: On behalf of all authors, the corresponding author states that there is no conflict of interest.

κ_0	Noise	$E(\mathbf{a}^0)$	$E(\hat{\mathbf{a}})$	$G(\mathbf{a}^0)$	$G(\hat{\mathbf{a}})$	$\|\nabla G(\mathbf{a}^0)\|_2$	$\|\nabla G(\hat{\mathbf{a}})\|_2$	#iter	#feval	Time	$G_{\zeta\equiv 1}(\hat{\mathbf{a}})$
13	2.89	20.55	13.43	0.50	0.06285	1.27564	0.11881	87	238	489.00	3.490e-08
13	2.89	22.39	12.79	0.50	0.04078	1.95351	0.06430	178	400	17862.53	4.329e-08
13	2.89	13.00	4.97	0.50	0.05157	1.88547	0.02771	211	470	21159.12	1.926e-08
13	2.89	17.74	16.42	0.50	0.10944	1.95232	0.73691	69	180	7482.35	1.175e-07
13	2.89	22.13	13.24	0.50	0.02336	1.80700	0.06277	103	255	10970.83	4.158e-08
13	2.89	18.73	11.64	0.50	0.01930	1.38184	0.02183	199	456	21590.15	2.735e-08
13	**2.89**	**15.50**	**3.76**	**0.50**	**0.01661**	**1.65920**	**0.01365**	**205**	**482**	**21867.62**	**1.924e-08**
13	2.89	20.33	13.01	0.50	0.04214	1.46118	0.09023	59	158	6663.72	3.679e-08
13	2.89	15.23	16.27	0.50	0.04179	1.98155	0.05757	133	322	15123.02	4.598e-08
14	**2.90**	**10.44**	**3.43**	**0.50**	**0.10264**	**1.44940**	**0.13051**	**55**	**179**	**385.20**	**1.589e-08**
14	2.90	18.37	3.37	0.50	0.03417	1.53146	0.01793	77	190	10679.42	1.730e-08
14	2.90	11.17	5.26	0.50	0.09079	1.62372	0.10239	33	103	4652.08	1.967e-08
14	2.90	17.47	2.60	0.50	0.05677	2.06821	0.11010	60	196	8771.41	1.617e-08
14	2.90	13.47	6.04	0.50	0.02708	2.07065	0.01264	90	239	13045.20	1.817e-08
14	2.90	9.98	5.81	0.50	0.04811	1.74643	0.04226	49	129	7022.91	1.843e-08
14	2.90	9.77	5.14	0.50	0.17494	1.50279	0.17384	58	156	8366.47	2.021e-08
14	2.90	10.09	6.02	0.50	0.19330	1.84977	0.11049	41	102	5916.89	1.977e-08
14	2.90	13.40	5.03	0.50	0.02962	2.24646	0.02551	45	113	6556.95	2.017e-08

Table 4: Results of using ten different initial points in the process of optimizing instances of the conductivity problem with internal measurements, $\kappa_0 \in \{13, 14\}$, and equidistant $\sigma^\star$.

Author contributions: All authors contributed equally to all phases of the development of this work.

Data availability: The datasets generated during and/or analyzed during the current study are available at `https://github.com/Souza-DR/bls2024-conductivity`.

Funding: This work has been partially supported by FAPESP (grants 2013/07375-0, 2022/05803-3, 2022/16733-6, and 2023/08706-1) and CNPq (grant 302073/2022-1). Antoine Laurain also acknowledges the support, since May 2023, of the Collaborating Researcher Program of the Institute of Mathematics and Statistics at the University of São Paulo.

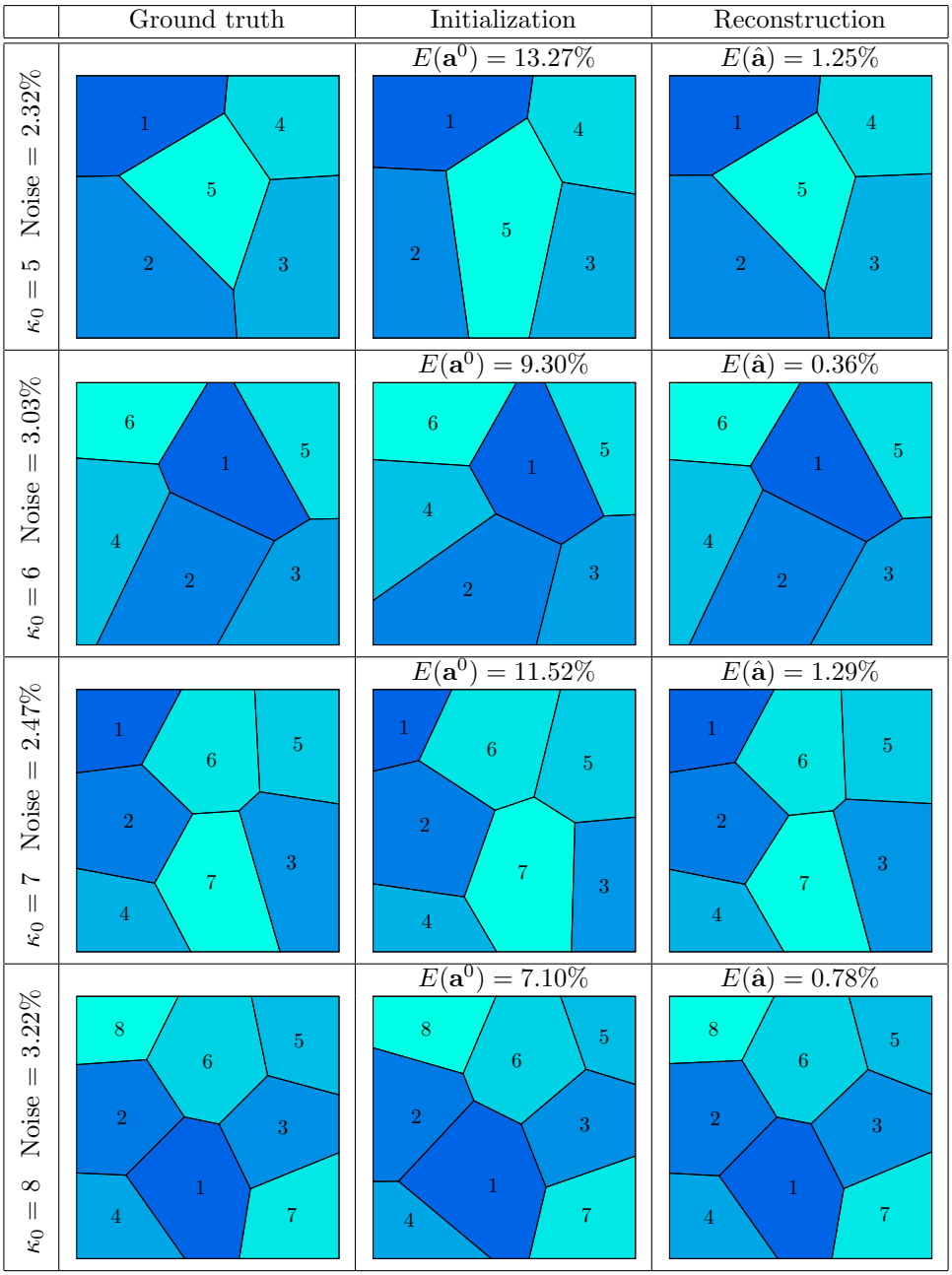

Figure 3: Graphical representation of solutions found for instances of the conductivity problem with internal measurements, $\kappa_0 \in \{5, 6, 7, 8\}$, and equidistant $\sigma^\star$. As a starting point, ten different ground truth perturbations were considered. For each of the ten initial points, the optimization process was performed. The solution with the lowest value of $G_{\zeta \equiv 1}(\hat{\mathbf{a}})$ among the ten solutions is reported in this figure.

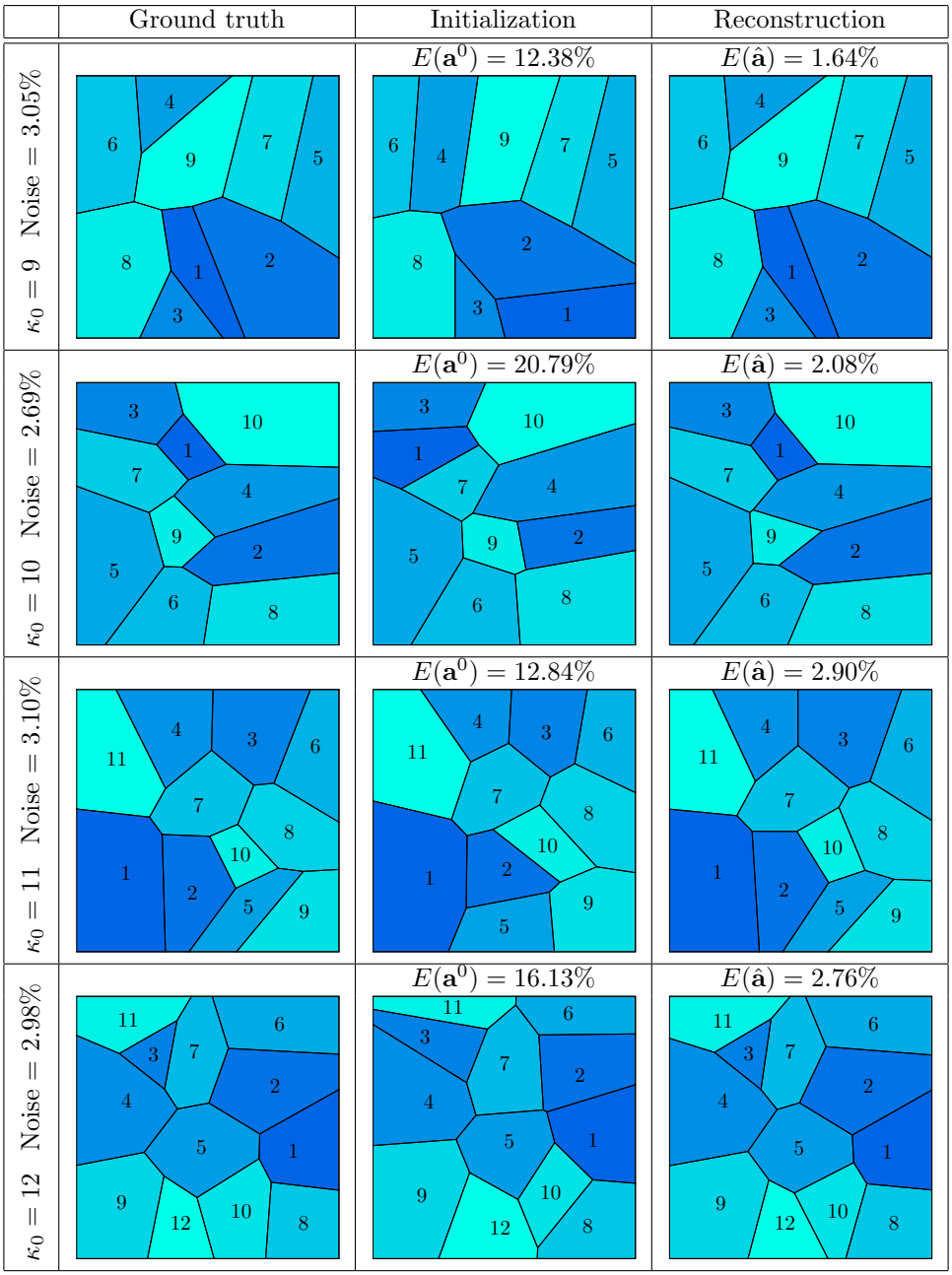

Figure 4: Graphical representation of solutions found for instances of the conductivity problem with internal measurements, $\kappa_0 \in \{9, 10, 11, 12\}$, and equidistant $\sigma^\star$. As a starting point, ten different ground truth perturbations were considered. For each of the ten initial points, the optimization process was performed. The solution with the lowest value of $G_{\zeta \equiv 1}(\hat{\mathbf{a}})$ among the ten solutions is reported in this figure.

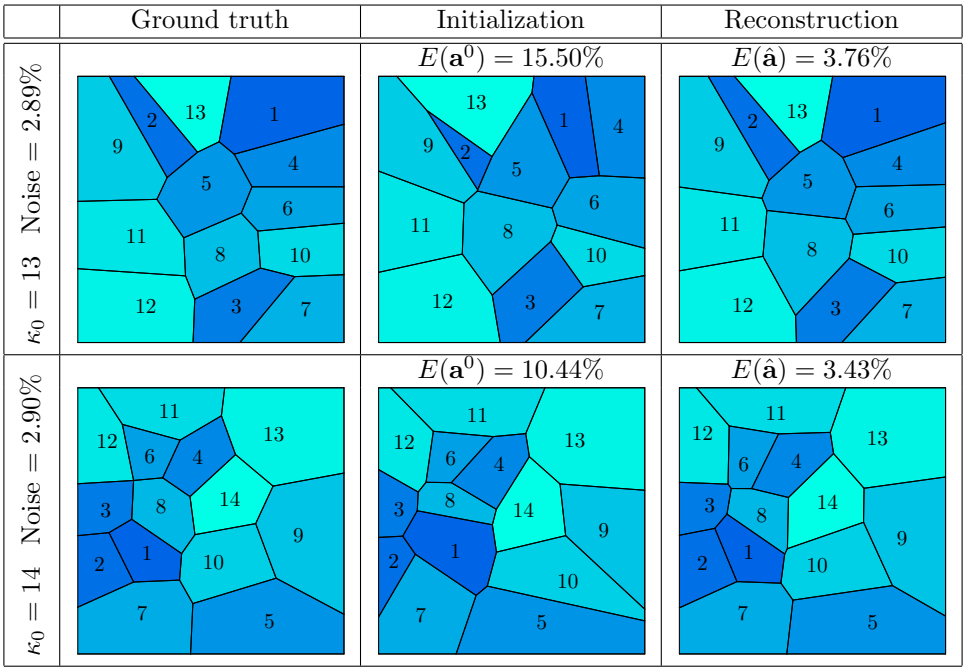

Figure 5: Graphical representation of solutions found for instances of the conductivity problem with internal measurements, $\kappa_0 \in \{13, 14\}$, and equidistant $\sigma^\star$. As a starting point, ten different ground truth perturbations were considered. For each of the ten initial points, the optimization process was performed. The solution with the lowest value of $G_{\zeta\equiv 1}(\hat{\mathbf{a}})$ among the ten solutions is reported in this figure.

κ_0	Noise	$E(\mathbf{a}^0)$	$E(\hat{\mathbf{a}})$	$G(\mathbf{a}^0)$	$G(\hat{\mathbf{a}})$	$\|\nabla G(\mathbf{a}^0)\|_2$	$\|\nabla G(\hat{\mathbf{a}})\|_2$	#iter	#feval	Time	$G_{\zeta\equiv 1}(\hat{\mathbf{a}})$
9	0.00	20.69	19.20	0.50	0.00059	1.49325	0.00528	109	302	13490.77	1.095e-07
	0.00	14.11	20.83	0.50	0.00290	1.81081	0.10915	115	289	14468.53	2.166e-07
	0.00	18.49	6.87	0.50	0.00034	1.85430	0.01603	57	160	1514.02	2.575e-08
	0.00	17.75	19.87	0.50	0.00112	1.24957	0.00812	110	291	14552.49	2.084e-07
	0.00	12.38	10.63	0.50	0.00100	1.90085	0.01255	115	275	14478.44	7.536e-08
	0.00	**12.37**	**4.72**	**0.50**	**0.00070**	**1.79104**	**0.02275**	**116**	**283**	**14423.01**	**4.925e-09**
	0.00	13.85	7.99	0.50	0.00063	2.05734	0.07946	114	281	14478.30	1.289e-08
	0.00	17.60	6.64	0.50	0.00580	2.56375	0.05070	115	275	14425.31	5.447e-08
	0.00	17.84	12.31	0.50	0.04928	1.98596	0.84315	116	299	14550.73	8.348e-08
	0.00	13.98	9.98	0.50	0.00651	1.79156	0.38681	116	273	14411.68	9.192e-08
9	0.37	20.69	21.06	0.50	0.00084	1.49353	0.00607	55	131	14606.83	1.559e-07
	0.37	14.11	26.23	0.50	0.05043	1.81098	0.86530	56	132	14522.53	3.773e-06
	0.37	18.49	6.60	0.50	0.00019	1.85479	0.01548	57	143	14522.14	1.481e-08
	0.37	17.75	19.18	0.50	0.00209	1.24960	0.01384	53	126	14471.93	3.889e-07
	0.37	12.38	13.30	0.50	0.00179	1.90089	0.05280	55	126	14597.96	1.350e-07
	0.37	**12.37**	**5.38**	**0.50**	**0.00196**	**1.78791**	**0.13449**	**56**	**124**	**14410.34**	**1.383e-08**
	0.37	13.85	10.89	0.50	0.00251	2.05716	0.08039	52	122	14441.49	5.127e-08
	0.37	17.60	6.72	0.50	0.00701	2.57003	0.06360	55	131	14474.25	6.554e-08
	0.37	17.84	13.46	0.50	0.05923	1.98629	1.49077	57	144	14618.80	1.012e-07
	0.37	13.98	10.28	0.50	0.00893	1.78929	0.09559	56	132	14479.43	1.266e-07
9	0.74	20.69	20.43	0.50	0.00079	1.49380	0.00410	54	132	14430.64	1.456e-07
	0.74	14.11	21.38	0.50	0.00216	1.81113	0.01869	55	133	14523.42	1.615e-07
	0.74	**18.49**	**7.47**	**0.50**	**0.00026**	**1.85526**	**0.01024**	**55**	**129**	**14430.02**	**1.975e-08**
	0.74	17.75	22.26	0.50	0.00102	1.24962	0.04309	53	121	14591.56	1.894e-07
	0.74	12.38	12.19	0.50	0.00154	1.90089	0.01375	55	125	14404.56	1.157e-07
	0.74	12.37	5.98	0.50	0.00425	1.78469	0.14621	56	137	14540.93	3.007e-08
	0.74	13.85	10.91	0.50	0.00258	2.05688	0.05396	52	130	14601.09	5.301e-08
	0.74	17.60	6.74	0.50	0.00749	2.57654	0.07019	55	130	14527.62	6.984e-08
	0.74	17.84	13.67	0.50	0.06408	1.98673	1.58814	56	137	14547.79	1.108e-07
	0.74	13.98	10.51	0.50	0.00941	1.78695	0.09402	56	134	14581.12	1.343e-07
9	1.48	20.69	19.56	0.50	0.00075	1.49432	0.00429	53	123	14526.01	1.380e-07
	1.48	14.11	20.42	0.50	0.00399	1.81136	0.03503	54	134	14483.71	2.992e-07
	1.48	18.49	8.45	0.50	0.00076	1.85619	0.04700	56	130	14476.60	5.803e-08
	1.48	17.75	17.73	0.50	0.00343	1.24966	0.03752	52	118	14478.70	6.401e-07
	1.48	12.38	13.09	0.50	0.00185	1.90084	0.01423	53	122	14613.06	1.396e-07
	1.48	**12.37**	**5.49**	**0.50**	**0.00497**	**1.77801**	**0.07882**	**56**	**134**	**14629.78**	**3.552e-08**
	1.48	13.85	10.25	0.50	0.00293	2.05606	0.34238	52	118	14586.15	6.055e-08
	1.48	17.60	6.77	0.50	0.00934	2.58481	0.06106	54	131	14427.43	8.656e-08
	1.48	17.84	14.06	0.50	0.07080	1.98689	0.86912	55	149	14606.08	1.267e-07
	1.48	13.98	10.39	0.50	0.00907	1.78211	0.07990	55	136	14504.87	1.310e-07

Table 5: Details of the optimization process of instances of the inverse conductivity problem with boundary measurements (EIT), $\kappa_0 = 9$, equidistant $\sigma_i^\star$, and $\bar{\alpha} = 1$. Four noise levels were considered with $c \in \{0.0, 0.0025, 0.005, 0.01\}$ as the standard deviation parameter of the normal Gaussian noise. As starting point of the optimization process, ten different ground truth perturbations were considered.

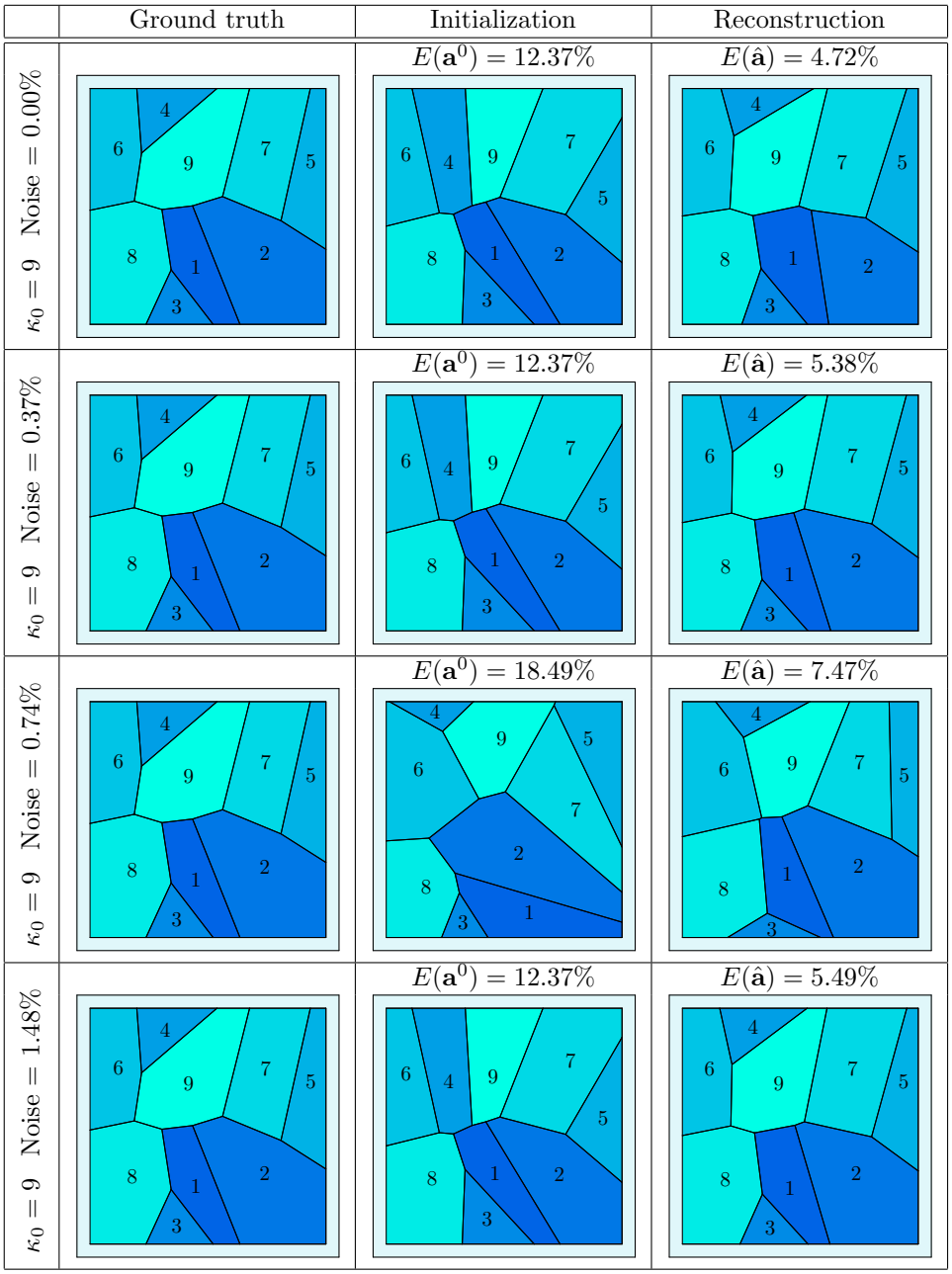

Figure 6: Graphical representation of solutions found for instances of the inverse conductivity problem with boundary measurements (EIT), $\kappa_0 = 9$, equidistant $\sigma_i^\star$, and $\bar{\alpha} = 1$. Notice the presence of the thin boundary layer Ω_0 in this problem, compare with Figure 1. Four noise levels were considered with $c \in \{0.0, 0.0025, 0.005, 0.01\}$ as the standard deviation parameter of the normal Gaussian noise. As a starting point, ten different ground truth perturbations were considered. For each of the ten initial points, the optimization process was performed. The solution with the lowest value of $G_{\zeta\equiv 1}(\hat{\mathbf{a}})$ among the ten solutions is reported in this figure.

κ_0	Noise	$E(\mathbf{a}^0)$	$E(\hat{\mathbf{a}})$	$G(\mathbf{a}^0)$	$G(\hat{\mathbf{a}})$	$\|\nabla G(\mathbf{a}^0)\|_2$	$\|\nabla G(\hat{\mathbf{a}})\|_2$	#iter	#feval	Time	$G_{\zeta\equiv 1}(\hat{\mathbf{a}})$
9	0.00	20.69	8.91	1.50	0.00149	1.84273	0.02414	137	323	43275.82	2.234e-07
	0.00	14.11	7.70	1.50	0.00260	2.02049	0.06024	135	320	43488.66	1.797e-07
	0.00	18.49	3.27	1.50	0.00034	1.92826	0.00824	139	321	43395.14	4.275e-08
	0.00	17.75	12.22	1.50	0.00229	1.46566	0.03871	135	291	43392.04	3.479e-07
	0.00	12.38	9.77	1.50	0.00179	2.39166	0.02079	135	316	43279.50	1.251e-07
	0.00	12.37	3.20	1.50	0.00197	1.76478	0.07176	139	310	43484.77	3.020e-08
	0.00	13.85	4.63	1.50	0.00117	2.41552	0.03156	138	328	43227.29	3.623e-08
	0.00	17.60	2.99	1.50	0.00160	2.54720	0.10741	139	317	43482.93	7.247e-08
	0.00	17.84	4.96	1.50	0.02193	2.11237	0.58281	140	352	43481.12	2.861e-07
	0.00	**13.98**	**3.48**	**1.50**	**0.00102**	**1.82756**	**0.10038**	**138**	**317**	**43399.82**	**1.821e-08**
9	0.39	20.69	12.03	1.50	0.00182	1.84156	0.01291	106	242	33899.66	2.834e-07
	0.41	14.11	8.11	1.50	0.00334	2.02382	0.10730	135	306	43325.11	2.376e-07
	0.45	18.49	3.45	1.50	0.00053	1.93105	0.01507	140	314	43425.96	7.108e-08
	0.41	17.75	11.53	1.50	0.00094	1.46375	0.00967	133	307	43241.74	1.580e-07
	0.41	12.38	9.35	1.50	0.00184	2.39224	0.02961	135	319	43275.75	1.279e-07
	0.40	12.37	3.21	1.50	0.00365	1.76904	0.08020	140	299	43345.77	5.448e-08
	0.41	13.85	4.61	1.50	0.00213	2.42190	0.11112	140	326	43460.94	6.169e-08
	0.42	17.60	2.63	1.50	0.00133	2.55103	0.13593	139	341	43395.70	6.412e-08
	0.40	17.84	3.09	1.50	0.00639	2.10844	0.34126	141	344	43364.62	9.961e-08
	0.44	**13.98**	**3.43**	**1.50**	**0.00194**	**1.82777**	**0.19277**	**140**	**315**	**43465.01**	**3.765e-08**
9	0.79	20.69	11.64	1.50	0.00229	1.84017	0.00670	80	195	26351.34	3.365e-07
	0.81	14.11	8.04	1.50	0.00438	2.02809	0.03609	141	324	43412.80	3.014e-07
	0.89	18.49	3.31	1.50	0.00089	1.93381	0.01008	145	346	43305.13	1.185e-07
	0.82	17.75	11.17	1.50	0.00135	1.46154	0.01413	138	311	43282.35	2.159e-07
	0.83	12.38	9.04	1.50	0.00259	2.38828	0.03591	143	328	43402.48	1.754e-07
	0.81	12.37	2.96	1.50	0.00708	1.77349	0.10515	145	338	43425.55	1.082e-07
	0.82	13.85	4.60	1.50	0.00445	2.42726	0.07455	105	269	33355.06	1.226e-07
	0.83	17.60	3.35	1.50	0.00386	2.55483	0.15252	145	344	43363.86	1.657e-07
	0.80	17.84	3.24	1.50	0.01282	2.10408	0.75484	145	361	43223.72	1.936e-07
	0.88	**13.98**	**3.86**	**1.50**	**0.00491**	**1.83122**	**0.05147**	**145**	**319**	**43435.91**	**1.005e-07**
9	1.58	20.69	10.70	1.50	0.00463	1.83676	0.02209	53	137	17714.48	6.221e-07
	1.62	14.11	7.79	1.50	0.00671	2.03953	0.15738	137	322	43210.21	4.496e-07
	1.79	18.49	3.83	1.50	0.00267	1.93925	0.02297	144	329	43461.54	3.566e-07
	1.65	17.75	12.49	1.50	0.00802	1.45633	0.10066	143	313	43225.89	1.175e-06
	1.66	12.38	9.76	1.50	0.00665	2.37681	0.03209	138	325	43343.10	4.480e-07
	1.63	12.37	3.09	1.50	0.02116	1.78275	0.10141	143	330	43324.74	3.417e-07
	1.64	13.85	4.31	1.50	0.01337	2.42319	0.10950	140	358	42834.43	3.583e-07
	1.67	17.60	4.91	1.50	0.01195	2.56226	0.16121	143	349	43408.14	5.060e-07
	1.60	17.84	5.68	1.50	0.06209	2.09417	1.13798	146	375	43282.10	8.141e-07
	1.76	**13.98**	**3.84**	**1.50**	**0.01576**	**1.84483**	**0.07556**	**142**	**317**	**43292.95**	**3.283e-07**

Table 6: Details of the optimization process of instances of the inverse conductivity problem with boundary measurements (EIT), $\kappa_0 = 9$, equidistant $\sigma_i^\star$, and $\bar{\alpha} = 3$. Four noise levels were considered with $c \in \{0.0, 0.0025, 0.005, 0.01\}$ as the standard deviation parameter of the normal Gaussian noise. As starting point of the optimization process, ten different ground truth perturbations were considered.

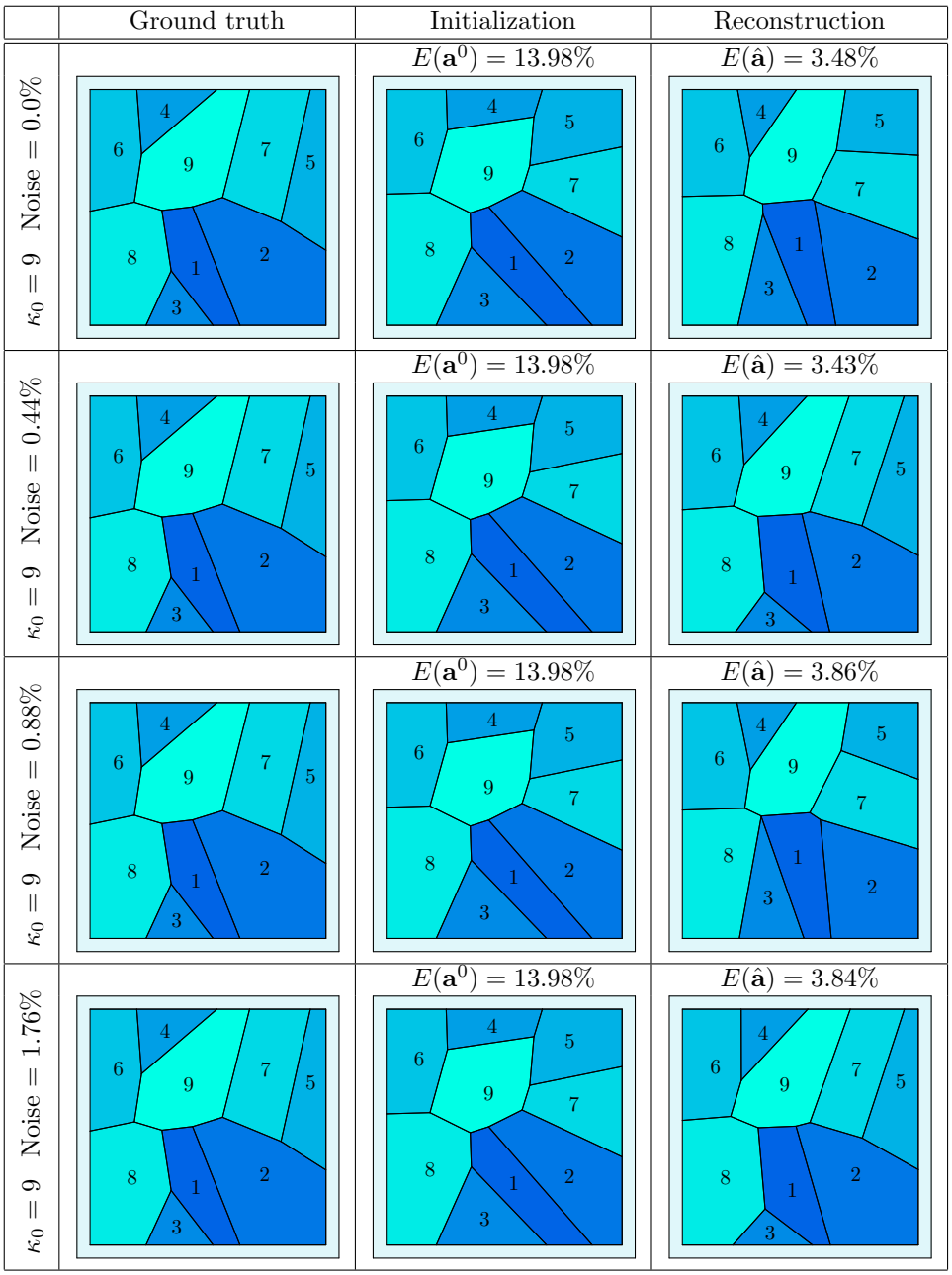

Figure 7: Graphical representation of solutions found for instances of the inverse conductivity problem with boundary measurements (EIT), $\kappa_0 = 9$, equidistant $\sigma_i^\star$, and $\bar{\alpha} = 3$. Four noise levels were considered with $c \in \{0.0, 0.0025, 0.005, 0.01\}$ as the standard deviation parameter of the normal Gaussian noise. As a starting point, ten different ground truth perturbations were considered. For each of the ten initial points, the optimization process was performed. The solution with the lowest value of $G_{\zeta\equiv 1}(\hat{\mathbf{a}})$ among the ten solutions is reported in this figure.

Appendix

We recall [37, Theorem 2.8], which is an application of the implicit function theorem suited for shape optimization problems with PDE constraints. We refer to [37] for the proof.

Assumption 4. *Let $\Omega \in \mathbb{P}(\mathcal{D})$, $E = E(\Omega), F = F(\Omega)$ be two Banach spaces with F reflexive, and consider a parameterization Ω_t defined by (21) for $t \in [0, t_1]$ for some $t_1 > 0$ and $\theta \in \mathcal{C}^{0,1}_{\partial\mathcal{D}}(\mathcal{D}, \mathbb{R}^d)$. Let $\mathfrak{L} : [0, t_1] \times E \times F \to \mathbb{R}$ be defined as*

$$\mathfrak{L}(t, \varphi, \psi) := \langle \mathcal{A}(t, \varphi), \psi \rangle_{F^*,F} + \mathcal{B}(t, \varphi), \tag{72}$$

where

$$\mathcal{A} : [0, t_1] \times E \to F^* \qquad \text{and} \qquad \mathcal{B} : [0, t_1] \times E \to \mathbb{R},$$

with $\mathcal{A} \in \mathcal{C}^1([0, t_1] \times E, F^*)$ and F^* is the dual of F. Let $u \in E$ be such that $\mathcal{A}(0, u) = 0$ and $\mathcal{B} : [0, t_1] \times E \to \mathbb{R}$ be differentiable at $(0, u)$. Denote by $A(u) := \partial_\varphi \mathcal{A}(0, u) \in \mathcal{L}(E, F^*)$, $L(u) := \partial_s \mathcal{A}(0, u) \in F^*$ and $B(u) := \partial_\varphi \mathcal{B}(0, u) \in E^*$.

Theorem 8. *Suppose that Assumption 4 holds and the linear operator $A(u) : E \to F^*$ is an isomorphism. Then, there exists $t_0 \in (0, t_1]$ and a unique $\mathcal{C}^1$ function $[0, t_0] \ni s \mapsto u^s \in E$ such that $u^0 = u$ and $\mathcal{A}(t, u^t) = 0$ for all $t \in [0, t_0]$. Also, the derivative $\dot{u} \in E$ of $t \mapsto u^t$ at $t = 0$ exists and $\dot{u} \in E$ is the unique solution of*

$$A(u)\dot{u} = -L(u) \in F^*. \tag{73}$$

Furthermore, let $\theta \in \mathcal{C}^{0,1}_{\partial\mathcal{D}}(\mathcal{D}, \mathbb{R}^d)$, T be the associated mapping satisfying Assumption 1, Ω_t defined in (21), and suppose that

$$J(\Omega_t) = \mathfrak{L}(t, u^t, \psi) \quad \text{for all } \psi \in F(\Omega). \tag{74}$$

Then under the above assumptions the shape derivative of $J(\Omega)$ in direction θ is given by

$$dJ(\Omega)(\theta) = \partial_t \mathfrak{L}(0, u, p) = \langle L(u), p \rangle_{F^*,F} + \partial_t \mathcal{B}(0, u), \tag{75}$$

where the adjoint state $p \in F$ is the unique solution of

$$A(u)^* p = -B(u) \in E^*, \tag{76}$$

and $A(u)^* : F \to E^*$ is the adjoint of $A(u) : E \to F^*$.

Proof of Theorem 5

Proof. In this proof we write $\mathbf{\Omega}$ instead of $\mathbf{\Omega}(\mathbf{a})$ for simplicity. Let $\mathcal{V}_i$ be the set of vertices of the cell $\Omega_i(\mathbf{a})$, then we either have $v = Y_{ijk}(0)$ if $v \in \mathcal{V}_i$ is an interior vertex, or $v = X_{ij\ell}(0)$ if $v \in \mathcal{V}_i$ is a boundary vertex (with respect to $\partial\mathcal{D}_0$), see Section 3.2. Define $\theta_v := \frac{d}{dt} Y_{ijk}(0)$ if $v \in \mathcal{V}_i$ is an interior vertex or $\theta_v := \frac{d}{dt} X_{ij\ell}(0)$ if $v \in \mathcal{V}_i$ is a boundary vertex. Using [13, Theorem 7] we know that

$$\theta_v = M_v(j, k, i)\delta a_i + M_v(k, i, j)\delta a_j + M_v(i, j, k)\delta a_k \tag{77}$$

if $v \in \mathcal{V}_i$ is an interior vertex. Here, (i, j, k) denote the indices of the three cells of the vertex v.

If v is a boundary vertex which is not a singular point of $\partial\mathcal{D}_0$, then θ_v is tangential to $\partial\mathcal{D}_0$, and we have

$$\theta_v = \mathscr{M}^\ell_v(j, i)\delta a_i + \mathscr{M}^\ell_v(i, j)\delta a_j, \tag{78}$$

see [13, Theorem 8]. Here (i, j) are the two indices of the cells of the vertex v and φ_ℓ are the level set functions representing the edges of $\partial\mathcal{D}_0$, see Section 3.2. If v is a boundary vertex which is also a singular point of $\partial\mathcal{D}_0$, then $\theta_v = 0$.

Next, introduce $\theta : \mathcal{D} \to \mathbb{R}^2$ defined as

$$\theta(x) := \sum_{v \in \mathcal{V}} \theta_v \psi_v(x). \tag{79}$$

By definition of ψ_v, one has $\theta \in W^{1,\infty}(\mathcal{D}, \mathbb{R}^2)$. Thanks to Assumption 2, one can show that the mapping $T(x,t) = x + t\theta(x)$, $x \in \mathcal{D}$, where θ is defined by (79), is bi-Lipschitz and valid to use in Theorem 1, see the proof of [14, Theorem 5]. We have $\theta = \partial_t T(\cdot, 0)$.

Thus, using Theorem 1 we have $G(\mathbf{a} + t\delta\mathbf{a}) = \mathfrak{J}(\mathbf{\Omega}(\mathbf{a} + t\delta\mathbf{a})) = \mathfrak{J}(T(\mathbf{\Omega}, t))$, hence

$$\nabla G(\mathbf{a}) \cdot \delta\mathbf{a} = \frac{d}{dt}(\mathfrak{J}(\mathbf{\Omega}(\mathbf{a} + t\delta\mathbf{a})))|_{t=0} = d\mathfrak{J}(\mathbf{\Omega})(\theta).$$

Next, we compute, in view of (79), $D\theta = \sum_{v\in\mathcal{V}} \theta_v \otimes \nabla\psi_v$ and

$$S_1(\mathbf{\Omega}) : D\theta = \sum_{v\in\mathcal{V}} S_1(\mathbf{\Omega}) : (\theta_v \otimes \nabla\psi_v) = \sum_{v\in\mathcal{V}} S_1(\mathbf{\Omega})\nabla\psi_v \cdot \theta_v.$$

This yields, using Theorem 3,

$$\begin{aligned} d\mathfrak{J}(\mathbf{\Omega})(\theta) &= \int_{\mathcal{D}} S_1(\mathbf{\Omega}) : D\theta + S_0(\mathbf{\Omega}) \cdot \theta \, dx = \sum_{v\in\mathcal{V}} \theta_v \cdot \int_{\mathcal{D}} S_1(\mathbf{\Omega})\nabla\psi_v(x) + S_0(\mathbf{\Omega})\psi_v(x) \, dx \\ &= \sum_{v\in\mathcal{V}} \theta_v \cdot \int_{\mathrm{supp}(\psi_v)} S_1(\mathbf{\Omega})\nabla\psi_v(x) + S_0(\mathbf{\Omega})\psi_v(x) \, dx. \end{aligned} \tag{80}$$

Thus we have obtained

$$\nabla G(\mathbf{a}) \cdot \delta\mathbf{a} = d\mathfrak{J}(\mathbf{\Omega})(\theta) = \sum_{v\in\mathcal{V}^{int}} \theta_v \cdot I(v) + \sum_{v\in\mathcal{V}^{bd}} \theta_v \cdot I(v).$$

Finally, using (77) and (78) we obtain (52). □

References

[1] L. Afraites, M. Dambrine, and D. Kateb. On second order shape optimization methods for electrical impedance tomography. *SIAM Journal on Control and Optimization*, 47(3):1556–1590, 2008.

[2] G. Alessandrini. An identification problem for an elliptic equation in two variables. *Annali di Matematica Pura ed Applicata. Serie Quarta*, 145:265–295, 1986.

[3] H. Ammari, J. Garnier, V. Jugnon, and H. Kang. Stability and resolution analysis for a topological derivative based imaging functional. *SIAM Journal on Control and Optimization*, 50(1):48–76, 2012.

[4] H. Ammari and H. Kang. *Reconstruction of small inhomogeneities from boundary measurements*, volume 1846 of *Lecture Notes in Mathematics*. Springer-Verlag, Berlin, 2004.

[5] G. Bal and G. Uhlmann. Reconstruction of coefficients in scalar second-order elliptic equations from knowledge of their solutions. *Communications on Pure and Applied Mathematics*, 66(10):1629–1652, 2013.

[6] B. Barceló, E. Fabes, and J. K. Seo. The inverse conductivity problem with one measurement: uniqueness for convex polyhedra. In *Partial differential equations of elliptic type (Cortona, 1992)*, volume XXXV of *Sympos. Math.*, pages 113–121. Cambridge Univ. Press, Cambridge, 1994.

[7] T. K. Bera. Applications of electrical impedance tomography (EIT): A short review. *IOP Conference Series: Materials Science and Engineering*, 331:012004, 2018.

[8] E. Beretta, S. Micheletti, S. Perotto, and M. Santacesaria. Reconstruction of a piecewise constant conductivity on a polygonal partition via shape optimization in EIT. *Journal of Computational Physics*, 353:264–280, 2018.

[9] Elena Beretta, Elisa Francini, and Sergio Vessella. A transmission problem on a polygonal partition: regularity and shape differentiability. *Applicable Analysis*, 98(10):1862–1874, 2019.

[10] D. P. Bertsekas. On the goldstein-levitin-polyak gradient projection method. *IEEE Transactions on Automatic Control*, 21(2):174–184, 1976.

[11] E. G. Birgin, A. Laurain, R. Massambone, and A. G. Santana. A shape optimization approach to the problem of covering a two-dimensional region with minimum-radius identical balls. *SIAM Journal on Scientific Computing*, 43(3):A2047–A2078, 2021.

[12] E. G. Birgin, A. Laurain, R. Massambone, and A. G. Santana. A shape-Newton approach to the problem of covering with identical balls. *SIAM Journal on Scientific Computing*, 44(2):A798–A824, 2022.

[13] E. G. Birgin, A. Laurain, and T. C. Menezes. Sensitivity analysis and tailored design of minimization diagrams. *Mathematics of Computation*, 92(344):2715–2768, 2023.

[14] E. G. Birgin, A. Laurain, and D. R. Souza. Reconstruction of Voronoi diagrams in inverse potential problems. *ESAIM: Control, Optimisation and Calculus of Variations*, 30:article 85, 2024.

[15] E. G. Birgin, J. M. Martínez, and M. Raydan. Nonmonotone spectral projected gradient methods on convex sets. *SIAM Journal on Optimization*, 10(4):1196–1211, 2000.

[16] M. Bonnet. Higher-order topological sensitivity for 2-D potential problems. Application to fast identification of inclusions. *International Journal of Solids and Structures*, 46(11-12):2275–2292, 2009.

[17] L. Borcea. Electrical impedance tomography. *Inverse Problems*, 18(6):R99–R136, 2002.

[18] E. T. Chung, T. F. Chan, and X.-C. Tai. Electrical impedance tomography using level set representation and total variational regularization. *Journal of Computational Physics*, 205(1):357–372, 2005.

[19] M. C. Delfour and J.-P. Zolésio. *Shapes and geometries*, volume 22 of *Advances in Design and Control*. Society for Industrial and Applied Mathematics (SIAM), Philadelphia, PA, second edition, 2011.

[20] R. S. Falk. Error estimates for the numerical identification of a variable coefficient. *Mathematics of Computation*, 40(162):537–546, 1983.

[21] A. Friedman and V. Isakov. On the uniqueness in the inverse conductivity problem with one measurement. *Indiana University Mathematics Journal*, 38(3):563–579, 1989.

[22] A. A. Goldstein. Convex programming in hilbert space. *Bulletin of the American Mathematical Society*, 70(5):709–710, 1964.

[23] P. Grisvard. *Elliptic problems in nonsmooth domains*, volume 24 of *Monographs and Studies in Mathematics*. Pitman (Advanced Publishing Program), Boston, MA, 1985.

[24] D. N. Hào and T. N. T. Quyen. Convergence rates for Tikhonov regularization of coefficient identification problems in Laplace-type equations. *Inverse Problems*, 26(12):125014, 23, 2010.

[25] B. Harrach. Recent progress on the factorization method for electrical impedance tomography. *Computational and Mathematical Methods in Medicine*, pages Art. ID 425184, 8, 2013.

[26] B. Harrach and M. Ullrich. Monotonicity-based shape reconstruction in electrical impedance tomography. *SIAM Journal on Mathematical Analysis*, 45(6):3382–3403, 2013.

[27] F. Hettlich and W. Rundell. The determination of a discontinuity in a conductivity from a single boundary measurement. *Inverse Problems*, 14(1):67–82, 1998.

[28] M. Hintermüller and A. Laurain. Electrical impedance tomography: from topology to shape. *Control and Cybernetics*, 37(4):913–933, 2008.

[29] M. Hintermüller, A. Laurain, and A. A. Novotny. Second-order topological expansion for electrical impedance tomography. *Adv. Comput. Math.*, 36(2):235–265, 2012.

[30] R. Hiptmair, A. Paganini, and S. Sargheini. Comparison of approximate shape gradients. *BIT*, 55(2):459–485, 2015.

[31] M. Ikehata and S. Siltanen. Numerical method for finding the convex hull of an inclusion in conductivity from boundary measurements. *Inverse Problems*, 16(4):1043–1052, 2000.

[32] V. Isakov. *Inverse problems for partial differential equations*, volume 127 of *Applied Mathematical Sciences*. Springer, Cham, third edition, 2017.

[33] R. Kohn and M. Vogelius. Determining conductivity by boundary measurements. *Communications on Pure and Applied Mathematics*, 37(3):289–298, 1984.

[34] P. D. Lamberti and L. Provenzano. On trace theorems for Sobolev spaces. *Matematiche (Catania)*, 75(1):137–165, 2020.

[35] H. P. Langtangen and A. Logg. *Solving PDEs in Python: The FEniCS Tutorial I*. Simula SpringerBriefs on Computing. Springer International Publishing, 2017.

[36] A. Laurain. Distributed and boundary expressions of first and second order shape derivatives in nonsmooth domains. *Journal de Mathématiques Pures et Appliquées*, 134:328–368, 2020.

[37] A. Laurain, P. T. P. Lopes, and J. C. Nakasato. An abstract Lagrangian framework for computing shape derivatives. *ESAIM. Control, Optimisation and Calculus of Variations*, 29:article 5, 2023.

[38] A. Laurain and K. Sturm. Distributed shape derivative *via* averaged adjoint method and applications. *ESAIM. Mathematical Modelling and Numerical Analysis*, 50(4):1241–1267, 2016.

[39] E. S. Levitin and B. T. Polyak. Constrained minimization methods. *USSR Computational Mathematics and Mathematical Physics*, 6(5):1–50, 1966.

[40] A. Logg, K.-A. Mardal, and G. N. Wells, editors. *Automated Solution of Differential Equations by the Finite Element Method*, volume 84 of *Lecture Notes in Computational Science and Engineering*. Springer, 2012.

[41] D. Mercier. Minimal regularity of the solutions of some transmission problems. *Mathematical Methods in the Applied Sciences*, 26(4):321–348, 2003.

[42] S. Nicaise. *Polygonal interface problems*, volume 39 of *Methoden und Verfahren der Mathematischen Physik [Methods and Procedures in Mathematical Physics]*. Verlag Peter D. Lang, Frankfurt am Main, 1993.

[43] S. Nicaise and A.-M. Sändig. General interface problems. I, II. *Mathematical Methods in the Applied Sciences*, 17(6):395–429, 431–450, 1994.

[44] G. R. Richter. An inverse problem for the steady state diffusion equation. *SIAM Journal on Applied Mathematics*, 41(2):210–221, 1981.

[45] J. Sokołowski and J.-P. Zolésio. *Introduction to shape optimization*, volume 16 of *Springer Series in Computational Mathematics*. Springer-Verlag, Berlin, 1992. Shape sensitivity analysis.

[46] F. Triki and T. Yin. Inverse conductivity problem with internal data. *Journal of Computational Mathematics*, 41(3):483–502, 2023.

[47] G. Uhlmann. Electrical impedance tomography and Calderón's problem. *Inverse Problems*, 25(12):123011, 39, 2009.

[48] S. Zhu. Effective shape optimization of Laplace eigenvalue problems using domain expressions of Eulerian derivatives. *Journal of Optimization Theory and Applications*, 176(1):17–34, 2018.